# Advanced methods to improve speed and accuracy of an iterative scattering radiative transfer solver


submitted by

Jakob Simon Dörr


Bachelor thesis in Meteorology

MIN-Fakultät

Universität Hamburg

October 5, 2016


1st Supervisor: Prof. Dr. Stefan Alexander Buehler

Meteorologisches Institut, Universität Hamburg

2nd Supervisor: Dr. Manfred Brath

Meteorologisches Institut, Universität Hamburg

**Thema der Arbeit**

Convergence acceleration for radiative transfer with scattering

**Abstract**

In this thesis, two methods are developed and implemented to optimize the 1-dimensional version of the DOIT (Discrete Ordinate ITerative) scattering solver. DOIT is part of the Atmospheric Radiative Transfer Simulator (ARTS). It is a very general solver which can handle many different situations. However, there are a few problems. One problem is that the calculations are slow in atmospheres with a lot of scattering. Another problem is that DOIT shows considerable differences to other scattering solvers which are implemented in ARTS. The first method aims at accelerating the convergence of DOIT in order to reduce computation time. The second method aims at increasing the accuracy of DOIT by optimizing the pressure grid of the calculations based on the properties of the atmosphere. Both methods are described and tested in this thesis.

The convergence acceleration speeds up the calculations by about 10% in the test cases. In atmospheres with a lot of ice and snow, it can double the speed of the calculation. Accelerating does not change the results of the calculations. The pressure grid optimization decreases the differences to the other solvers to around 1 K. This comes at the cost of higher calculation time.

# Contents

# List of Figures

# 1 Introduction

Radiative transfer describes the interaction of radiation with the particles in the atmosphere. It is a very important subject in many science disciplines, especially in the field of remote sensing. In remote sensing, it is necessary to be able to simulate radiative transfer. This can be used for example to extract information about the atmosphere from radiation measurements of radiometers. There are many radiometers which measure atmospheric radiation in the microwave and sub-millimeter spectral range. For example, the Advanced Microwave Sounding Unit B (AMSU-B, Saunders et al. (1995)) measures in the microwave range and the Ice Cloud Imager (ICI), which will be on the new Meteorological Operational Satellite - Second Generation B (MetOp-SG B, Pica et al. (2012)) from 2022, measures in both the microwave and the sub-millimeter range.
In these spectral ranges, clouds, especially ice clouds, interact with the radiation mainly by scattering (Buehler et al., 2007). To simulate radiative transfer with clouds in this spectral range, it is therefore necessary to have a radiative transfer model which can calculate the effects of scattering.
The Atmospheric Radiative Transfer Simulator (ARTS, Eriksson et al. (2011); Buehler et al. (2005)) is such a model. It is a line-by-line radiative transfer code for thermal radiation.
To simulate the effects of scattering, three different scattering solvers are implemented in ARTS. ARTS-Monte-Carlo (ARTS-MC) by Davis et al. (2005) uses a backward Monte Carlo method to simulate the radiation. It is basically simulating the path of a number of photons in the medium. DISORT (Stamnes et al., 2000) is a DIScrete Ordinate Radiative Transfer code with 1-dimensional plane-parallel geometry and DOIT is a Discrete Ordinate ITerative scattering solver with spherical geometry by Emde et al. (2004). While ARTS-MC uses a rather stochastic approach, both DISORT and DOIT directly simulate radiative transfer on a discrete grid.
In addition to the scattering effect, the different applications of radiative transfer simulations pose other challenges to the models:

- For simulations of horizontally heterogeneous clouds, it is important to have a 3-dimensional model
- Some applications require the simulation of polarized radiation
- Measurements in limb directions (through the edge of the atmosphere) require a spherical geometry
- To derive other properties of the atmosphere, it is necessary to simulate the whole radiation field, not just a single path
- The calculations should be finished in a reasonable amount of time

No solver implemented in ARTS is currently able to fulfill all these requirements for radiative transfer with scattering. While DISORT works very efficiently and calculates the whole radiation field, it can only calculate 1-dimensional problems without polarization.

Furthermore, it cannot be used to simulate limb directions, as it assumes plane-parallel geometry. ARTS-MC can handle both 3-dimensional problems and polarization and it is suited for limb calculations. However, it can only calculate a single beam at a time, therefore showing very slow performance if the whole radiation field wants to be computed. DOIT, on the other hand, can also handle 1-dimensional as well as 3-dimensional problems and it calculates the whole radiation field. It can simulate polarized radiation and is also able to simulate limb directions, because it assumes a spherical geometry. Thus, DOIT is the most general of the three solvers.
However, the iterative method of the DOIT solver converges very slowly, depending on the difficulty of the problem. Furthermore, in some problems, it differs considerably from the other two solvers, while those agree at the same time.
The motivation of this thesis is to improve the DOIT solver so that it is faster and more accurate. This thesis presents two methods that both accelerate the convergence of the DOIT solver and optimize the calculations to ensure higher accuracy and reliability. Both methods are implemented into DOIT and tested with frequencies in the sub-millimeter and microwave spectral range.
Chapter 2 presents a short theoretical background on radiative transfer with scattering as well as basics about the DOIT method. The convergence acceleration and its implementation are described and tested in chapter 3. In chapter 4, the errors of DOIT are analysed and a pressure grid optimization and its implementation are described and tested.

# 2 Fundamentals

## 2.1 Radiative transfer with scattering

In this thesis, the radiative transfer of electromagnetic radiation in the mircowave and submillimeter spectral range is considered. The microwave range extends from 0.3 to 300 GHz in terms of the frequency of the radiation (Rees, 2012). The submillimeter range extends from about 300 to 3000 GHz, which corresponds to wavelength below 1 mm to 0.1 mm. This is consistent with literature, for example Evans et al. (2012) and Buehler et al. (2007). An overview of the electromagnetic spectrum and the range described here is given in Figure 1.

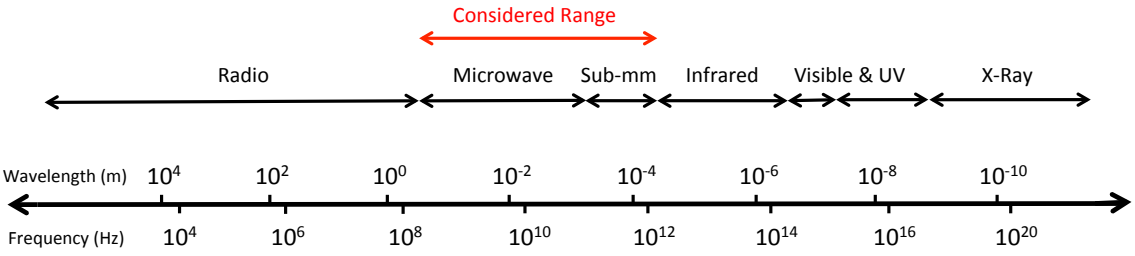


Figure 1: The electromagnetic spectrum and the range used in this thesis.

When radiation travels through matter, they interact. Along a ray of light, the radiation can be changed due to absorption, thermal emission and scattering (see Figure 2). Radiation is taken out of the ray if it hits a particle and gets absorbed. A particle can also emit radiation, according to Planck's law. This radiation is added to the ray. Radiation can also be scattered by particles. This can change the direction of the radiation. Thus, scattering can both increase and decrease the radiation of the ray, as light can be scattered into or scattered out of the ray.

A good measure of the radiation is the intensity (or spectral radiance) $I$ . The intensity is the energy of the radiation passing through a defined area $dA$ from a specific direction at a specific frequency $\nu$. It is defined by Rees (2012) as

$$I = \frac{dP}{dA\ cos\theta\ d\Omega\ d\nu} \tag{1}$$

where $dP$ is the power of the radiation, $\Omega$ is the solid angle and $\theta$ is the angle between the area normal and the radiation.

In remote sensing, the intensity is often replaced by the brightness temperature $T_b$. The brightness temperature is the temperature of a black body emitting radiation at this intensity and frequency. It can be calculated using Planck's law of thermal emission.

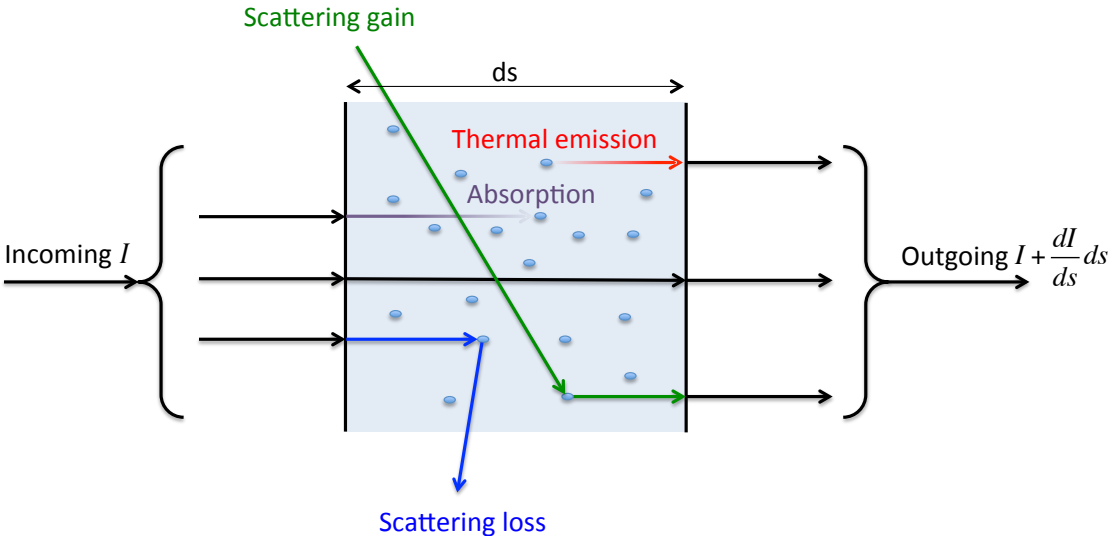


Figure 2: Visualization of the processes that characterize the interaction of radiation (Intensity $I$ with matter a long a path $ds$

The processes that change the radiation are described by the radiative transfer equation (RTE). It describes the change of the intensity along a ray of light. It can be written in a phenomenological way similar to Figure 2:

$$\begin{aligned}\text{Change of intensity} = &- (\text{Absorption} + \text{Scattering loss}) + \text{Thermal emission} \\ &+ \text{Scattering gain}\end{aligned}$$

Mathematically, in a medium with absorption, scattering and thermal emission, the RTE of unpolarized radiation is according to Mishchenko et al. (2002):

$$\begin{aligned}\frac{dI(\nu, T, \boldsymbol{n})}{ds} = &- (\alpha(\nu, T, \boldsymbol{n}) + \sigma(\nu, T, \boldsymbol{n}))I(\nu, T, \boldsymbol{n}) + \alpha(\nu, T, \boldsymbol{n})B(\nu, T) \\ &+ \sigma(\nu, T, \boldsymbol{n}) \int_{4\pi} Z(\nu, T, \boldsymbol{n}, \boldsymbol{n'})I(\nu, T, \boldsymbol{n})d\boldsymbol{n'}\end{aligned} \tag{2}$$

where $\alpha$ and $\sigma$ are the absorption and scattering coefficients respectively, $B$ is the Planck function and $Z$ is the scattering phase function. Furthermore $\nu$ is the frequency, $T$ the temperature, $ds$ is a path element and $\boldsymbol{n}$ the propagation direction of the ray. Note that $B$ is only equivalent to the Planck Function when local thermodynamic equilibrium (LTE) is assumed. In the following equations, LTE is assumed unless otherwise stated. The scattering phase function $Z$ of a particle describes the strength and direction of the scattered radiation, depending on the incoming radiation.

Equation 2 is a monochromatic equation as it is assumed that scattering does not change the frequency of the radiation in the context described here. This means, it can be solved separately for every frequency.

When polarization effects are also considered, equation 2 becomes the vector radiative

transfer equation (VRTE):

$$\frac{d\boldsymbol{I}(\nu,T,\boldsymbol{n})}{ds} = -\Big(\boldsymbol{\alpha}(\nu,T,\boldsymbol{n}) + \boldsymbol{\sigma}(\nu,T,\boldsymbol{n})\Big)\boldsymbol{I}(\nu,T,\boldsymbol{n}) + \boldsymbol{\alpha}(\nu,T,\boldsymbol{n})B(\nu,T) + \boldsymbol{\sigma}(\nu,T,\boldsymbol{n})\int_{4\pi}\boldsymbol{Z}(\boldsymbol{n},\boldsymbol{n'},\nu,T)\boldsymbol{I}(\boldsymbol{n'},\nu,T)d\boldsymbol{n'} \tag{3}$$

where $\boldsymbol{I}$ is the Stokes vector and $\boldsymbol{\alpha}$, $\boldsymbol{\sigma}$ and $\mathbf{Z}$ are matrices. The Stokes vector $\boldsymbol{I} = (I, Q, U, V)^\intercal$ is used to fully describe the radiation. $Q$ and $U$ describe the linear polarization and $V$ describes the circular polarization of the radiation. All parameters of the Stokes vector can be measured. Details on the Stokes vector can be found in Rees (2012). One can call the last term in equations 2 and 3 the scattering source function. In cases without scattering, $\sigma$ and the scattering source function vanish and equations 2 and 3 can be solved analytically with boundary conditions. This equation is also known as Schwarzschild's equation. In the considered spectral region, light is scattered mostly by cloud particles. This is why scattering can be neglected if there are no clouds in the atmosphere. Situations without scattering are therefore referred to as clear-sky cases.
In the presence of scattering, the equations cannot be solved analytically and instead have to be solved using numerical methods. The smaller the scattering $\sigma$ is in comparison to the absorption $\alpha$, the less difficult it will be to solve the equations. The DOIT program is able to solve the equations in the presence of scattering.

## 2.2 The DOIT method

The DOIT scattering solver (Emde et al., 2004) uses an iterative method to solve equations 2 and 3. The method works for polarized as well as for unpolarized radiation. For unpolarized radiation, equation 2 is solved and for polarized radiation, equation 3 is solved. In the following equations, the dependencies on the direction, the frequency and the temperature will be omitted for better readability.
The radiation in the atmosphere depends on the position (altitude, latitude, longitude) in the atmosphere and the viewing direction. All these dimensions are discretized on a grid. The special feature of ARTS and DOIT is that the calculations are performed on a spherical grid, i.e. on polar coordinates. Because DOIT is a scattering solver, it only needs to calculate radiative transfer where scattering is actually happening in the atmosphere. In the context of this thesis, it means where there are clouds in the atmosphere. The region where DOIT calculates radiative transfer is therefore called the cloudbox. By default, it is set so that it covers the region where there are scattering particles in the atmosphere. Calculations outside the cloudbox are done using the clear-sky calculations of ARTS.
The DOIT model geometry is visualized in Figure 3. In the cloudbox, the calculations are done on discrete spherical coordinates. For the 1-dimensional case this means that the atmosphere is divided vertically into a number of layers with different pressures $p$. Within these layers, the properties of the atmosphere are assumed to be constant. Furthermore,

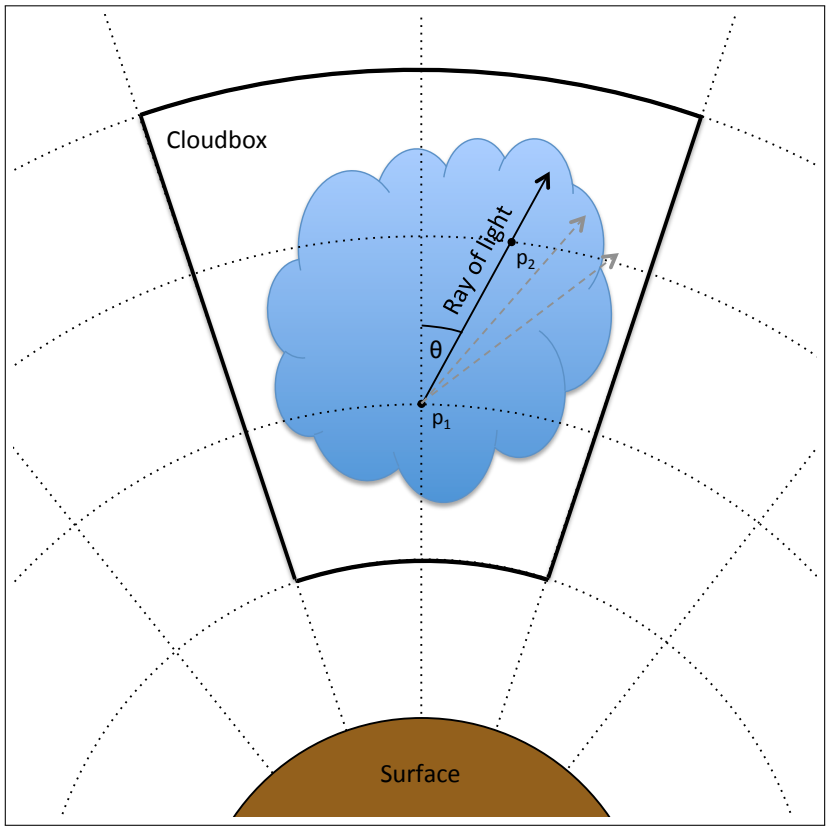


Figure 3: Geometry of DOIT and ARTS and an example of a light of ray passing from level $p_1$ through level $p_2$ of the cloudbox at a specific angle $\theta$. Other rays indicated by the grey dashed arrows

the calculations are performed on a discrete grid of zenith angles. Equations 2 and 3 are solved for a number of rays, covering every angle in the angle grid and therefore crossing the cloudbox in every possible direction. As the rays pass through the different homogeneous layers, they interact with the particles in the layers. The calculated intensity or the Stokes vector is stored for every layer and for every angle. This leads to a field of radiation. The calculations are performed several times in the iterative process, until the process has reached convergence.

The calculation is started with a first guess radiation field. This field can be set by the user. By default, it is calculated by interpolating the boundary conditions to the whole atmosphere.

Interpolation and other processing steps are omitted in the following explanation in order to focus on the essential method. Each iteration consists of two basic steps. The first step of the n-th iteration is to calculate the scattering integrals $S_{n-1}$ from the radiation field of the (n-1)-th iteration $I_{n-1}$ in every layer and for every angle. This leads to the scattering source function of the (n-1)-th iteration:

$$S_{n-1} = \sigma \int_{4\pi} Z I_{n-1} dn' \tag{4}$$

The integration itself is done on a discrete grid which consists of two angles.
For the second step, the scattering source function in equations 2 and 3 is assumed to be constant. It is replaced by $S_{n-1}$ which has been obtained in equation 4. This leads to the equation

$$\frac{dI_n}{ds} = -(\alpha + \sigma)I_n + \alpha B + S_{n-1} \tag{5}$$

where $I_n$ is the radiation field of the n-th iteration. This equation can now be solved using an exponential approach:

$$I_n = e^{-(\alpha+\sigma)s} I_{n-1} + \Big(1 - e^{-(\alpha+\sigma)s}\Big)(\alpha + \sigma)^{-1}\Big(\alpha B + S_{n-1}\Big) \tag{6}$$

where $I_{n-1}$ is the radiation field of the (n-1)-th iteration. This step is calculated along all the rays covering every angle. The intensity is stored for every layer and every angle to obtain the field $I_n$, which is used as the input for the next iteration.
This scheme is followed until the sequence $I_1, I_2, ..., I_n$ has reached convergence, meaning that the difference between the field of the n-th iteration and the (n-1)-th iteration is smaller than a defined threshold. The threshold can be given in intensity or in brightness temperatures. For more details on the iteration scheme, see Emde et al. (2004) and Eriksson et al. (2016). DOIT assumes LTE and single scattering. Single scattering means that the radiation is only scattered once in every layer.
Because this iterative method on spherical coordinates is a very general approach with few assumptions, it can be applied to many different problems. DOIT can calculate 1-dimensional as well as 3-dimensional problems, although 3-dimensional calculations are very slow. It can handle nadir as well as limb directions and it can calculate problems with arbitrarily oriented and shaped particles. One of the downsides however is its large computation time.

## 2.3 ARTS setup

To analyze the current state of DOIT and to test the implemented methods, radiative transfer calculations are performed with different atmospheric profiles. All radiative transfer calculations in this thesis are done using ARTS version 2.3. The frequencies used for the calculations correspond to the channels of the instruments ISMAR (International Sub-Millimetre Airborne Radiometer) and MARSS (Microwave Airborne Radiometer Scanning System). They are in the range of about 88 to 880 GHz. For details on the channels, see Fox et al. (2014).
To simulate gas absorption, the HITRAN (HIgh Resolution TRANsmission) database (Rothman et al., 2013) and the MT_CKD model for continuum absorption of water vapor and nitrogen in version 2.52 and for oxygen in version 1.00 (Mlawer et al., 2012) are used. The surface emissivity is calculated with the FASTEM (Fast Microwave Emissivity Model, Liu et al. (2011)) implementation in ARTS 2.3 using surface wind speed and surface temperature from the atmospheric profiles.

To simulate scattering in the atmosphere, four different cloud particles are added to the model: ice particles, snow flakes, rain drops and cloud drops. The particle size distributions and the scattering properties of the particles are calculated like Geer and Baordo (2014) and Hong et al. (2009). The particles are assumed to be spherical and their scattering properties are described by the Mie Theory (see Stratton (1941) for details), except for the snow flakes, which are assumed to behave like aggregates in the Hong-DDA (Discrete Dipole Approximation) data base (Hong et al., 2009).

# 3 Convergence acceleration

One of the issues of DOIT is its large computation time due to slow convergence in some cases. A slow convergence means that DOIT has to calculate many iterations to reach the convergence threshold. In this chapter, a method is presented that helps DOIT to converge faster. First, the current state of DOIT is analyzed with test data in order to understand in which cases DOIT is converging slowly. After that, the acceleration method and its implementation into DOIT is explained. The accelerated DOIT is then analyzed again in order to test the efficiency of the acceleration method, to understand in which cases it has the most effect and to check if it yields the same results as the original DOIT.

## 3.1 Current state of DOIT

To analyze the convergence behavior of DOIT, 1-dimensional radiative transfer calculations are performed in 375 atmospheres. The atmospheric data comes from model output of the regional version of the ICOsahedral Non-hydrostatic Model (ICON). For more information on ICON see Zängl et al. (2015) and Reinert et al. (2016). The output consists of atmospheric data over the ocean from the region between 50°N and 75°N and 30°W and 5°E on 11th, 13th and 18th march 2015. It has a gridded resolution of about 10 km. To generate 1-dimensional atmosphere sets, 375 vertical profiles are randomly selected from the model output.

Two sets of calculations are performed: one set in which the full Stokes vector $\boldsymbol{I}$ is computed, and one set in which only the intensity $I$ is computed, i.e. neglecting polarization. Furthermore, the calculations are performed on 44 different frequencies and on a grid of 62 pressure levels and 25 zenith angles.

The convergence thresholds are set to the same values in every calculation. Table 1 shows the convergence thresholds for the 4 components of the Stokes vector. The thresholds are chosen relative to the average size of the component. Because the last three components of $\boldsymbol{I}$ are much smaller than the first, their threshold is smaller.

Table 1: Convergence thresholds for the test calculations with DOIT

| $[\mathrm{Wm^{-2}sr^{-1}Hz^{-1}}]$ | $I$ | $Q$ | $U$ | $V$ |
|---|---|---|---|---|
| polarized | $1 \times 10^{-18}$ | $1 \times 10^{-19}$ | $1 \times 10^{-19}$ | $1 \times 10^{-19}$ |
| unpolarized | $1 \times 10^{-18}$ | - | - | - |

The number of iterations until convergence is counted for every atmosphere and frequency. The number of iterations it a good indicator for the speed of the calculation. This is because it determines the calculation time but it is robust because it does not depend on the speed of the processors.

Finally, additional calculations are performed using the DOIT method with a constant number of 100 iterations. This high number of iterations is used to ensure that the process has fully converged. In this context, these calculations will henceforth be called reference calculations.

According to Buehler et al. (2007), ice particles interact with radiation in the microwave and sub-millimeter spectral region mainly by scattering. Therefore the amount of snow and ice in an atmosphere should be a good indicator how fast DOIT converges in this atmosphere. A good measure for the amount of snow and ice is the IWP (Ice Water Path). It is defined as

$$IWP = \int_0^\infty (\rho_{ice}(z) + \rho_{snow}(z))dz \tag{7}$$

where $\rho_{ice}$ and $\rho_{snow}$ are the particle mass densities of ice and snow, respectively, and $z$ is the altitude.

Figure 4 shows that the average number of iterations per frequency in an atmosphere depends on the amount of snow and ice in this atmosphere. In atmospheres with little or no snow and ice, convergence is reached mostly after two iterations. After the amount of ice and snow has surpassed a certain value, the number of iterations rises to a maximum of over 14 iterations per frequency for both polarized and unpolarized radiation. The difference between polarized and unpolarized radiation is small. The convergence for polarized radiation is a little slower because the convergence threshold for the last three components of $\boldsymbol{I}$ is smaller than for $I$.

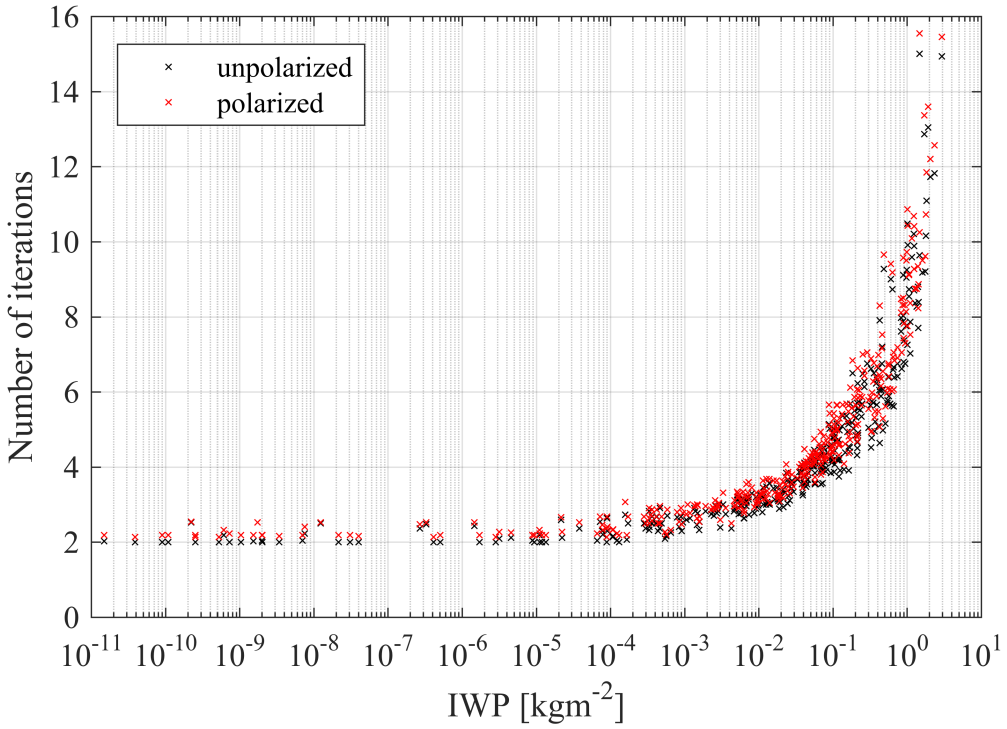


Figure 4: Average number of iterations of the DOIT method over 44 frequencies for 375 atmospheres against the IWP in the atmosphere for polarized and unpolarized radiation

When looking at the individual frequencies in Figure 5, it seems that DOIT generally needs more iterations to converge in higher frequencies. This is because the scattering of the particles is stronger in the higher frequencies. However, in a few higher frequencies, DOIT converges after very few iterations in every atmosphere. This is because these frequencies lie close to absorption lines of atmospheric gases. One example is the 183-GHz-line of water vapor, another is the 448-GHz-line of water vapor. Both are mentioned in Fox et al. (2014). The strong absorption of the gases overcompensates the strong scattering of the particles and DOIT converges quickly. In these frequencies, the number of iterations is similar in every atmosphere, as indicated by the difference of the average and the maximum. This means that the number of iterations is independent from the amount of scatterers in the atmosphere. In other frequencies, the number of iterations varies with the amount of scatterers. The pattern is similar in polarized and unpolarized radiation.
This means that DOIT takes many iterations to converge mainly in cases where the scattering is high compared to the absorption. For the tests, this is given if there is a lot of ice particles in the atmosphere.
In all calculations, the solution is compared to the reference calculation. One would expect that the converged solutions differ from the reference not more than the convergence threshold. However, in about 15% of the atmospheres, even though DOIT has converged with the given threshold, the maximum difference to the reference solution is bigger than this threshold. This happens predominantly in the frequencies where DOIT needs many iterations to converge. The reason for this is the slow convergence of DOIT in these cases. The decision if DOIT has converged or not is based on the difference of two succesive iterations. Because of the slow convergence in these cases, the difference between the iterations is already very small even though the current iteration is far from the actual solution.
One example can be seen in Figure 6. The maximum difference between the converged solution and the reference in this example is more than 3 times the threshold. This means that when using DOIT, a certain threshold does not necessarily lead to the accuracy of this threshold. To make sure he gets a certain accuracy, the user should choose a smaller threshold.
To sum up, DOIT only needs many iterations in cases where the scattering is high compared to the absorption. Furthermore, in some of these cases, the convergence is so slow that the solution is not close enough to the reference solution, even though it has converged according to the convergence threshold.

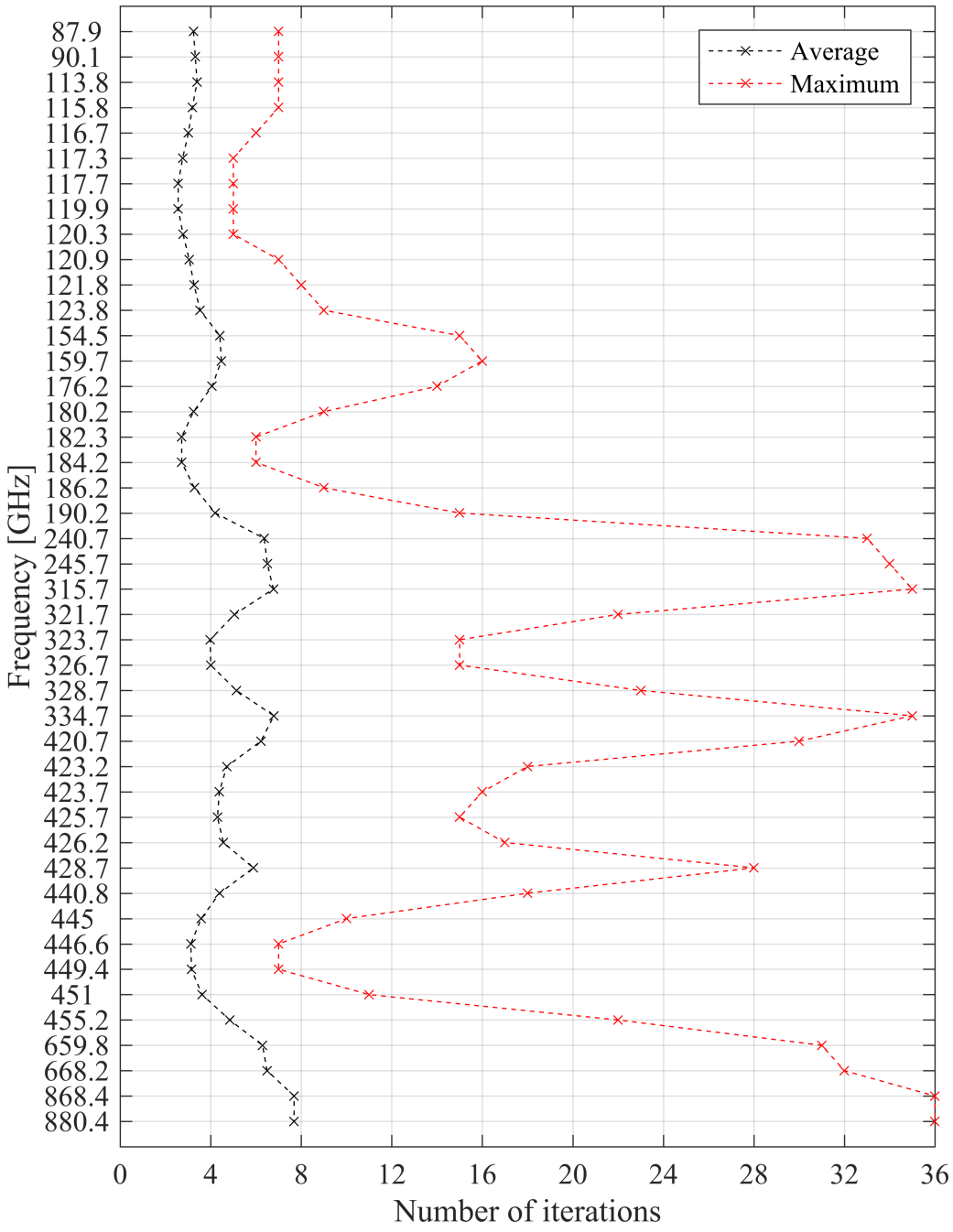


Figure 5: Average and maximum iterations of the DOIT method over all atmospheres with respect to the 44 frequences for unpolarized radiation

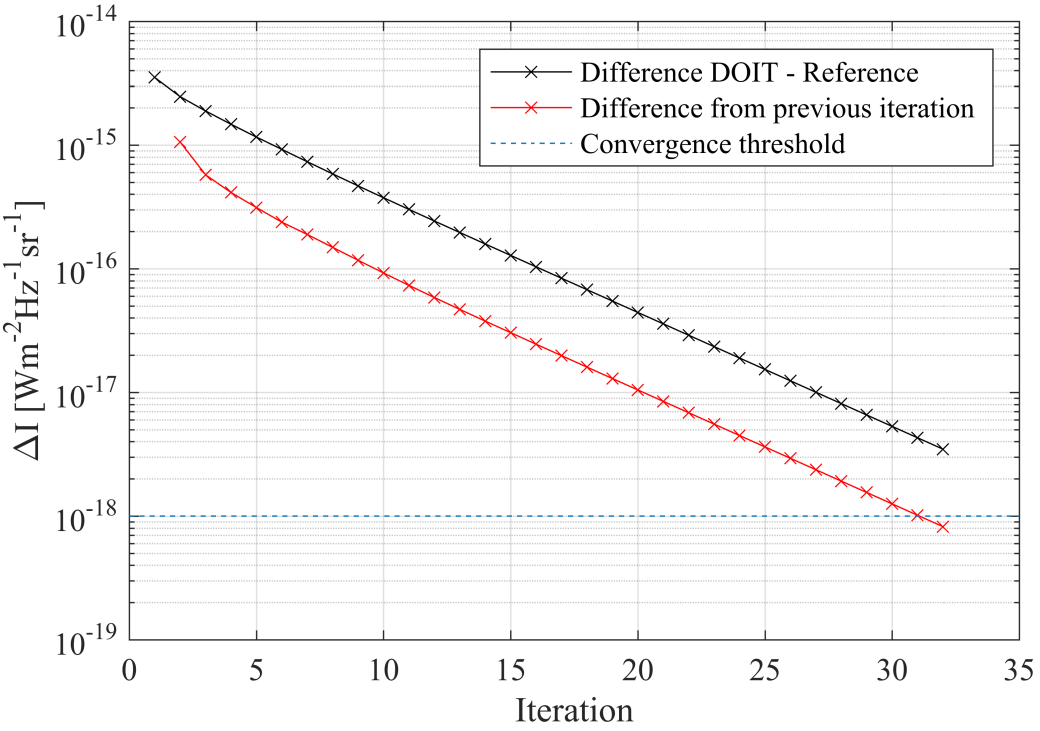


Figure 6: Maximum difference in the intensity of 32 successive iterations of the DOIT method to the reference calculation, combined with the maximum difference to the previous iteration, and the convergence threshold; unpolarized radiation, atmosphere no. 121, frequency 315.7 GHz

## 3.2 The acceleration method

The acceleration method that is implemented in DOIT is called the Ng-acceleration. This acceleration method was developed by Ng (1974). It has been used in the context of astrophysical radiative transfer (Olson et al., 1986; Pereira and Uitenbroek, 2015). This section briefly explains this method.
An iterative problem may generally be written in the form

$$f = Af, \tag{8}$$

where $f$ is a function to be computed and $A$ is a function operator. An example of such an operator is the derivative. The usual iteration procedure is to start with a first guess of $f$ and to calculate the $(n+1)$-th iteration of $f$, $f_{n+1}$, using equation 8

$$f_{n+1} = Af_n, \tag{9}$$

where $f_n$ is the $n$-th iteration. If the sequence $f_1, f_2, \ldots$ is converging, the converged element should be a solution to equation 8. This means that the difference between two successive iterations decreases as the process is approaching convergence.
The Ng-acceleration uses this property to extract information out of a number of given iterations and to calculate an estimated field that is closer to the solution. In this work, a version which uses the last 4 iterations is implemented. It is presented in the following.
Given the iterations $f_n, f_{n-1}, f_{n-2}$ and $f_{n-3}$, $\bar{f}_1$ is defined as

$$\bar{f}_1 = (1-a-b)f_{n-1} + af_{n-2} + bf_{n-3} \tag{10}$$

and its successor $\bar{f}_2$

$$\bar{f}_2 = (1-a-b)f_n + af_{n-1} + bf_{n-2}, \tag{11}$$

where $a$ and $b$ are some constants to be determined. Because $\bar{f}_2$ is the successor of $\bar{f}_1$, it follows from equation 9 that

$$\bar{f}_2 = A\bar{f}_1. \tag{12}$$

The difference $d$ between $\bar{f}_1$ and $\bar{f}_2$ is then defined by

$$d = \bar{f}_2 - \bar{f}_1 = A\bar{f}_1 - \bar{f}_1. \tag{13}$$

A good global measure of the difference d is

$$||d||_2 = \sqrt{\int_D d(x)^2 dx}, \tag{14}$$

where $D$ is the domain over which the calculations are performed and $x$ is the integration variable. This represents the $l_2$-Norm of $d$. For $\bar{f}_2$ to be very close to the converged solution, it should solve equation 8 in the best possible way, i.e. with a margin defined by the user. This means that the difference $d$ to $\bar{f}_1$ should be as small as possible. Therefore, it is necessary to minimize $||d||_2^2$ (the squared norm of $d$) using the constants $a$ and $b$. Minimizing $||d||_2^2$ with respect to $a$ and $b$ leads to two equations which can be used to solve for $a$ and $b$. Details of this calculation can be found in appendix A. The solution for $a$ and $b$ in the 4-iteration case is

$$a = \frac{(d_n, d_1)(d_2, d_2) - (d_n, d_2)(d_1, d_2)}{(d_1, d_2)(d_2, d_2) - (d_1, d_2)(d_1, d_2)} \tag{15}$$

$$b = \frac{(d_n, d_1)(d_1, d_2) - (d_n, d_2)(d_1, d_1)}{(d_1, d_2)(d_1, d_2) - (d_2, d_2)(d_1, d_1)} \tag{16}$$

with

$$(f, g) = \int_D f(x)g(x)dx \tag{17}$$

being the scalar product of the functions f and g which induces the norm $||\cdot||_2$ and

$$d_n = f_n - f_{n-1} \tag{18}$$
$$d_1 = f_n - 2f_{n-1} + f_{n-2} \tag{19}$$
$$d_2 = f_n - f_{n-1} - f_{n-2} + f_{n-3}. \tag{20}$$

The field

$$\bar{f}_2 = (1 - a - b)f_n + af_{n-1} + bf_{n-2} \tag{21}$$

will now be a good replacement of the $(n+1)$-th iteration. After an acceleration step, three normal iterations must be performed in order to acquire enough information for the next acceleration step.

This acceleration method can be adapted for different numbers of iterations in between the acceleration steps. The more iterations the method uses, the more information it can obtain. Therefore, the method will work better for more iterations in between the acceleration steps. However, the more iterations there are in between the acceleration steps, the lower the efficiency of the method will be. The choice to implement a version with 4 iterations is a trade-off between these two factors in order to maximize the efficiency.

### 3.3 Implementation in DOIT

Because the DOIT solver uses an iterative method to compute the radiation field, the Ng-acceleration can be applied. In this case, the function $f$ is the radiation field $I$ which is computed by DOIT. Mathematically, the equation that describes the iterative process of DOIT is a combination of equation 6 and equation 4:

$$\begin{aligned} I_n =& e^{-(\alpha+\sigma)s} I_{n-1} \\ &+ \Big(1 - e^{-(\alpha+\sigma)s}\Big)(\alpha+\sigma)^{-1}\Big(\alpha B + \sigma \int_{4\pi} Z I_{n-1} dn'\Big). \end{aligned} \tag{22}$$

Please note that there are interpolation steps in the actual calculations which have been omitted for the sake of clarity. This equation has the same form as equation 9. After every iteration, the radiation field $I_n$ of this iteration is stored. After every 4 iterations, the constants $a$ and $b$ and the accelerated field $I_{n+1}$ are computed. This field is then the input of the next iteration, if necessary (e.g. not converged yet). To accelerate calculations with polarization, the four components of $\boldsymbol{I}$ are accelerated seperately.

It is important to notice that the Ng-acceleration is not an approximation of the solution. Because three normal iterations are performed in between the acceleration steps, the accelerated version should always converge to the same solution than the non-accelerated version.

The acceleration method is only applied to the 1-dimensional version of DOIT. An expansion to the 3-dimensional version is not subject of this thesis as the 1-dimensional version is the most used. The acceleration is implemented in ARTS and can be controlled by the parameter *accelerated*, which can be set in the workspace method $doit\_i\_field\_monoIterate$. If no acceleration is wished, then *accelerated* should be set to 0. If acceleration is wished, then *accelerated* can be set from 1 to 4, depending on how many Stokes components are to be accelerated.

Figure 7 shows the effect of the acceleration method in an atmospheric scenario of the ICON data set. The non-accelerated method converges after 32 iterations while the accelerated converges after only 13 iterations. Every 4 iterations, the accelerated method jumps closer to the solution and reaches convergence earlier than the non-accelerated method. Both converge to the same solution, that is, they do not differ from each other more than the convergence threshold.

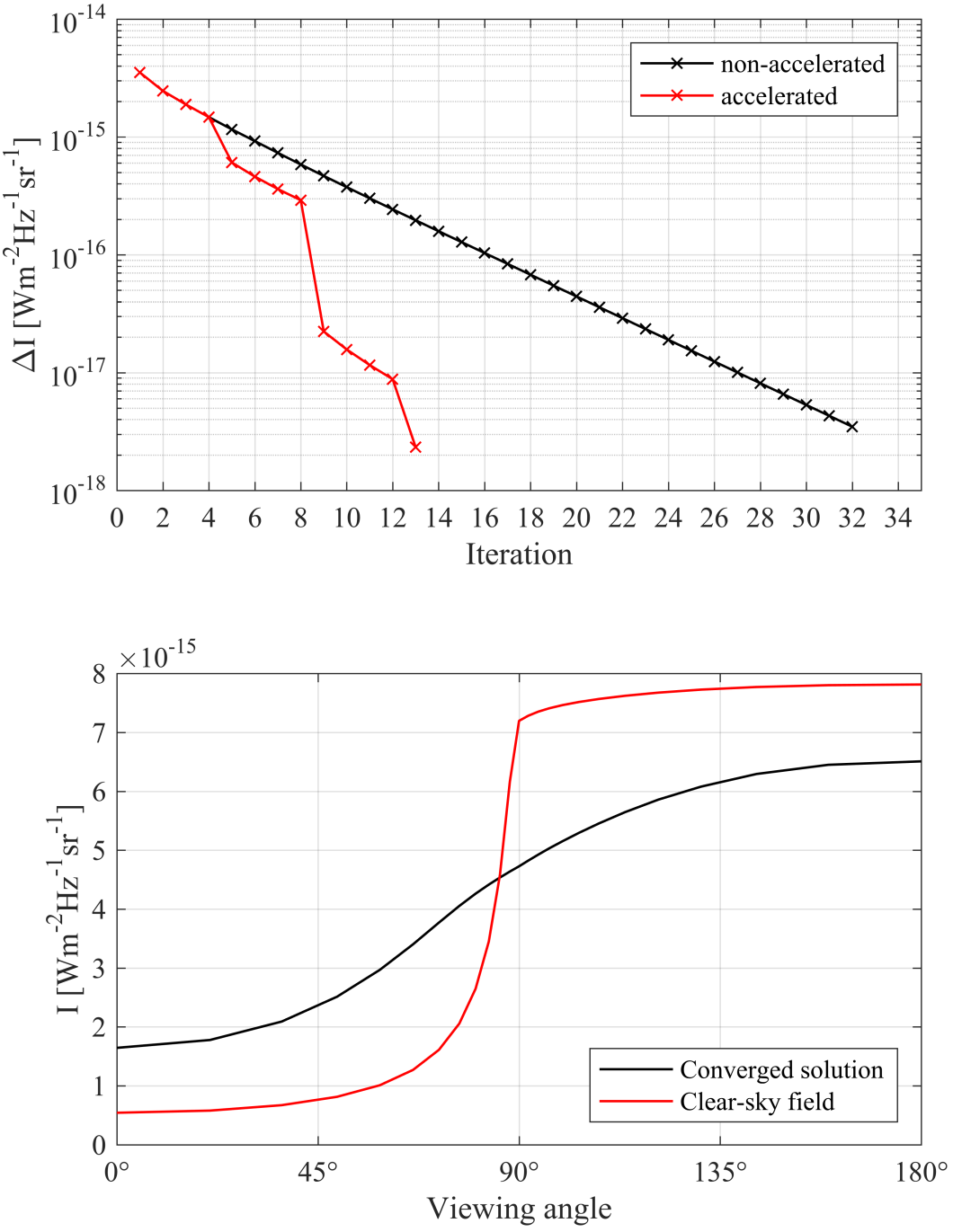


Figure 7: Maximum difference in the calculated intensity of the non-accelerated and accelerated version of DOIT to the reference calculation (top), reference solution with the corresponding clear-sky field, viewing position at 495 hPa (bottom); unpolarized radiation, atmosphere no. 121, Frequency 315.7 GHz

## 3.4 Testing and discussion

In this section, the accelerated DOIT method is tested. The comparison is done under the same conditions as for the original DOIT method. The calculations are also split into polarized and unpolarized radiation to see if the acceleration also works with polarization.

The average number of iterations over all frequencies and all atmospheres is lower for the accelerated version, both in polarized and unpolarized radiation. In unpolarized radiation, the accelerated version takes about 11% less iterations to converge, in polarized radiation about 9% less.
However, this difference is not equally distributed over the 375 atmospheres. The top part of Figure 8 shows that for unpolarized radiation and atmospheres with large amounts of ice and snow, the difference is much bigger than 11%, while in atmospheres with very little snow and ice, the accelerated and non-accelerated version converge after the same amount of iterations. This is because in these cases, the non-accelerated version typically converges after less than 4 iterations. Therefore, the Ng-acceleration, which has its first acceleration step after the 4th iteration, does not make a difference. Only when the non-accelerated version takes more than 5 iterations, the Ng-acceleration has a change to speed up the convergence. Figure 15 in appendix B shows a similar pattern for polarized radiation. If only those atmospheres are counted, where the non-accelerated version takes more than 5 iterations on average to converge, the accelerated version takes about 21% less iterations to converge for unpolarized radiation and about 17% for polarized radiation.
Above 5 iterations it can be said that the more iterations the non-accelerated version takes to converge, the more effective the Ng-acceleration gets. In the bottom part of Figure 8 it can also be seen that the acceleration shows the strongest effect in the maximum iterations per frequency. In some extreme cases, the accelerated version takes less than half the iterations of the non-accelerated version.
This can also be seen when looking at the individual frequencies. Figure 9 shows that for unpolarized radiation, the Ng-acceleration significantly reduces the maximum number of iterations. However, at frequencies where the maximum of the non-accelerated version is at or around 5 iterations, the acceleration has little or no effect. A similar pattern can be observed for polarized radiation in Figure 16 in appendix B. Hence, the largest part of the overall acceleration comes from reducing the maximums.
While the results show that the Ng-acceleration also works for polarized radiation, there are some small problems. For unpolarized radiation, the average number of iterations per frequency of the accelerated version is always lower than the non-accelerated version. However, for polarized radiation, the accelerated version sometimes takes more iterations per frequency than the non-accelerated. This is the case for only 11 of the 375 atmospheres, and the difference is very small, but it is worth mentioning. This could happen because the last three components of $\boldsymbol{I}$ show a convergence behavior that is difficult for the acceleration. This problem is very small and overcompensated by the acceleration in the other atmospheres and can therefore be neglected.

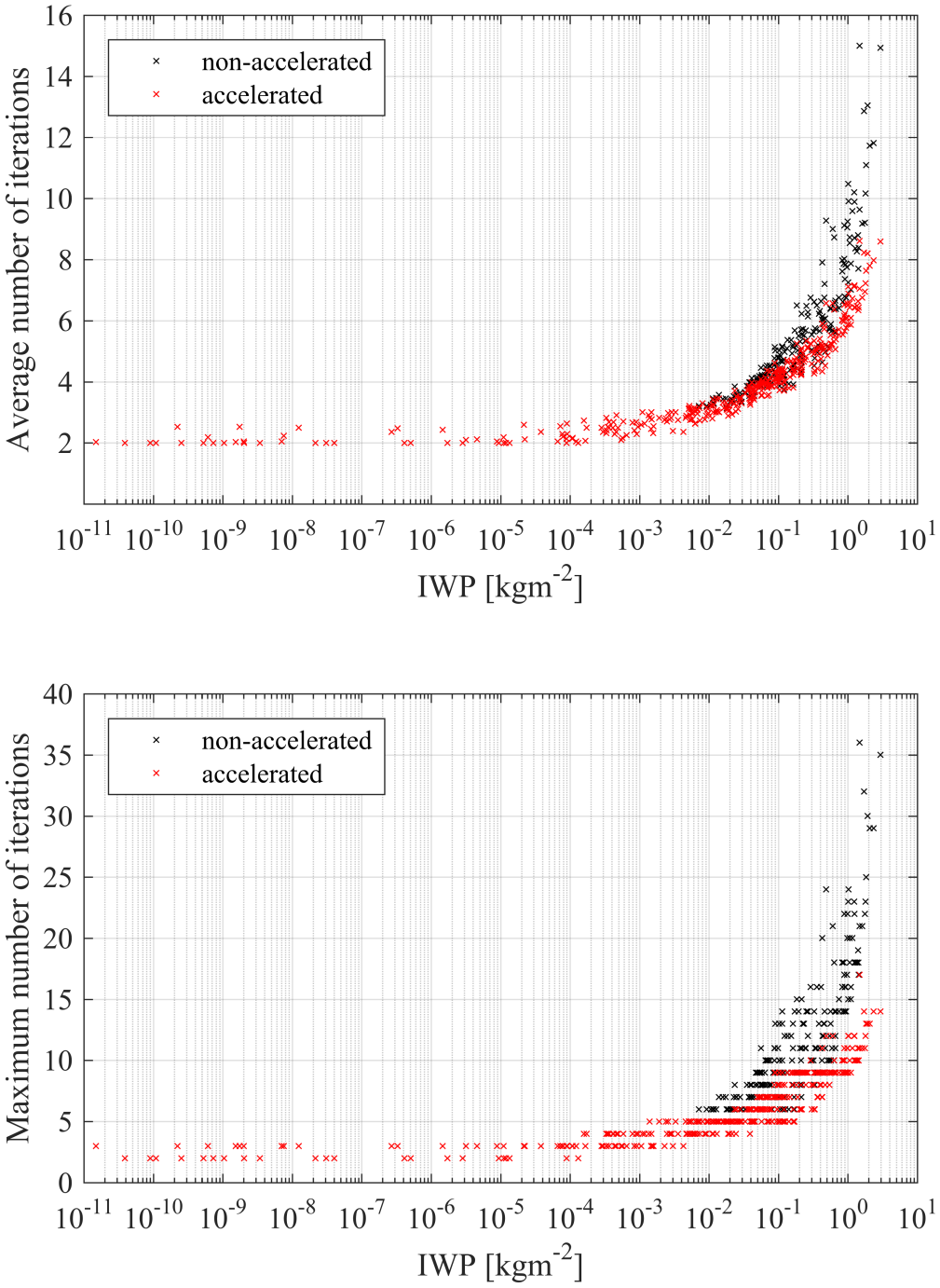


Figure 8: Number of iterations until convergence, for all atmospheres, average (top) and maximum (bottom) over all frequencies, for the non-accelerated and the accelerated version of DOIT against the IWP in the atmosphere; unpolarized radiation

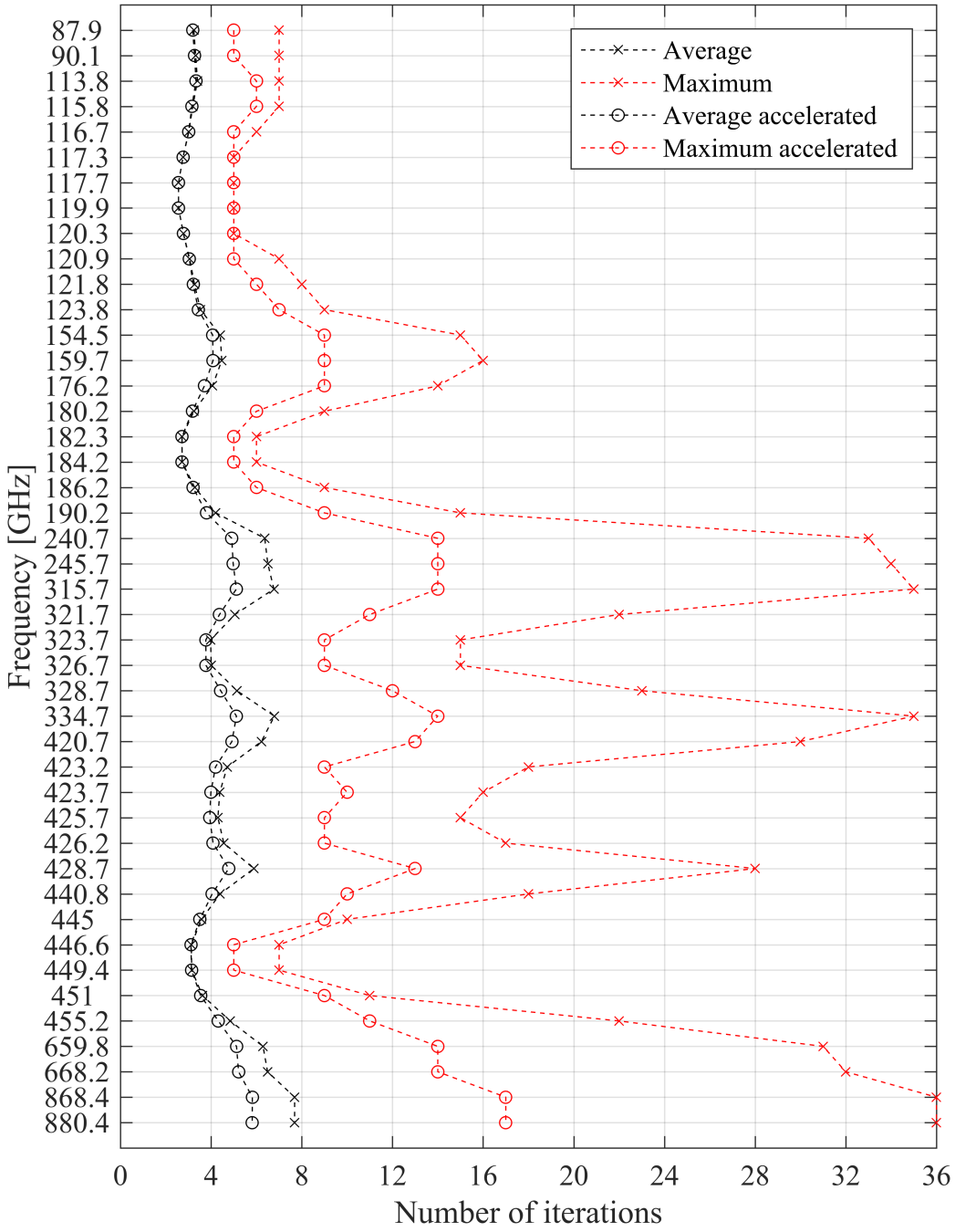


Figure 9: Average and maximum iterations over all atmospheres with respect to the frequency of the 44 channels for the accelerated and the non-accelerated version of DOIT, calculation with unpolarized radiation

To test if the accelerated version yields the same results as the original version, both solutions are compared to each other and to the reference calculation. For both polarized and unpolarized radiation, the solutions of the accelerated and the original DOIT method are similar within the convergence threshold. As written in section 3.1, in some cases, the solution from the non-accelerated version differs from the reference calculation to an extent larger than the convergence threshold. This problem is also observed with the accelerated version, but the number of such cases is significantly reduced, from 15 % of the atmospheres to about 5%. In all cases where the accelerated version shows a too large difference to the reference, the non-accelerated version has an equal or even larger difference. This means that in the test cases, the Ng-acceleration has no negative effect on the accuracy of the solution. It rather has a positive effect, as it increases the number of cases where the converged solution is close enough to the reference.
In summary, the Ng-acceleration is able to speed up DOIT by about 10% in the test cases. In atmospheres where DOIT takes more than 5 iterations to converge, the acceleration starts having an effect and the effect grows with the number of iteration that DOIT takes. While the convergence acceleration has some minor problems with polarized radiation, it does not change the solution of the calculations and can therefore safely be used to accelerate DOIT.

# 4 Pressure grid optimization

The DOIT solver assumes the single scattering approximation for the propagation path steps. This means that it assumes that the light is only scattered once within one model layer. According to Emde et al. (2004), this approximation is good if the layers are optically thin enough. This means that all layers have to have a rather small optical thickness. The optical thickness $\tau$ is defined as the integral of the extinction coefficient $\kappa = \alpha + \sigma$ over the propagation path step from $s_1$ to $s_2$:

$$\tau(s_1, s_2) = \int_{s_1}^{s_2} \kappa(s')ds'. \tag{23}$$

In a homogeneous layer which extents from $s_1$ to $s_2$, the optical thickness can be rewritten as

$$\tau(s_1, s_2) = \kappa(s_2 - s_1) \tag{24}$$

Emde et al. (2004) mentions that the user can define a limit for the maximum length of a path from one layer to the next. The idea is that the user can choose a small step length in order to avoid errors resulting from too large optical thicknesses. This feature, however, was never actually implemented in DOIT.

## 4.1 Analysis of the current state

To analyze the model errors, calculations from DISORT and ARTS-MC are compared to the original DOIT version. The test atmosphere in which the calculations are performed comes from the Chevallier data set by Chevallier et al. (2006). It contains a lot of ice and snow and can be seen as an extreme test case. The 26 frequencies on which the calculations are performed correspond to 13 different channels. Each channel is represented by two frequencies surrounding the channel's center frequency.
For the original DOIT version, a pressure grid with 56 grid points in the cloud box is used. The convergence threshold is set to 0.01 K in terms of brightness temperature to ensure that it fully converges. Furthermore, the angular grid is set to a very fine resolution to rule out errors that arise from a too coarse angular grid. ARTS-MC is set to an accuracy of 0.1 K and DISORT is set to 8 streams (see Stamnes et al. (2000) for more information). The calculations are done with unpolarized radiation.
To compare the results with those of the DISORT and ARTS-MC solvers, a virtual sensor is placed at 850 km above the surface, looking nadir (straight down) and 50° from nadir. The simulated brightness temperatures $T_b$ of the unpolarized radiation measured by this sensor are compared for every channel. Because DISORT also computes the radiation field, the brightness temperatures of DISORT and DOIT are compared at every pressure level for the nadir direction.

Figure 10 shows that the difference between the original DOIT and the other models is up to 6 K for some channels. At the same time, DISORT and ARTS-MC agree within their respective accuracy. Therefore it is necessary to implement an optimization of the pressure grid on which the DOIT calculations are performed.

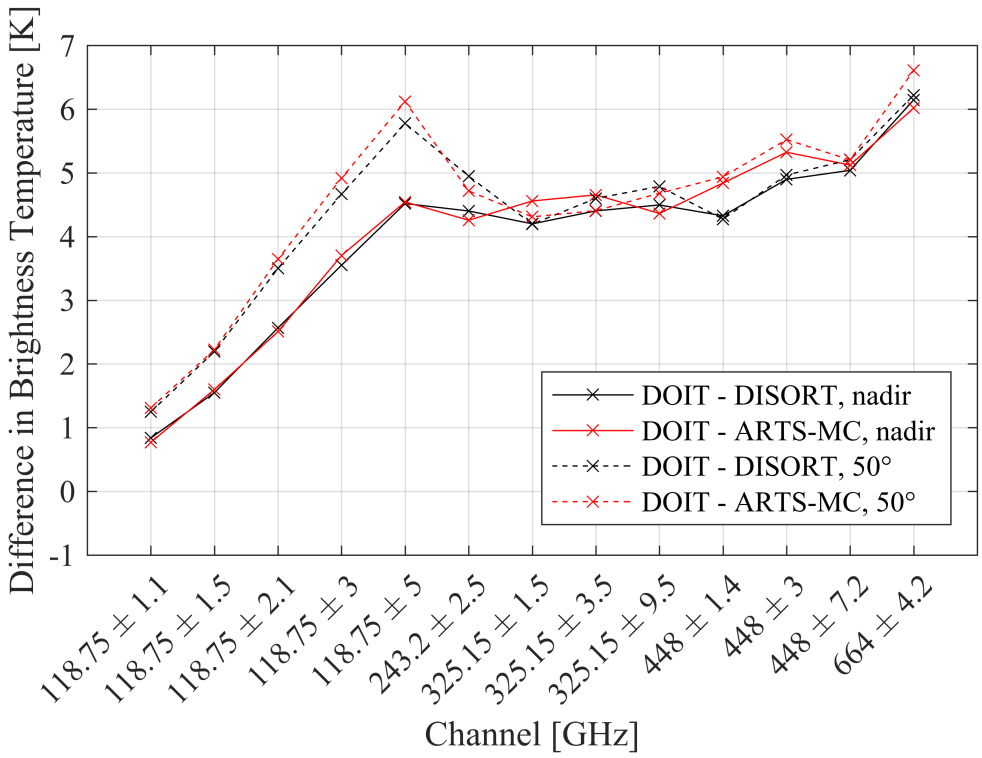


Figure 10: Difference of DOIT to DISORT and ARTS-MC in simulated measured brightness temperatures for 13 different channels

## 4.2 Optimization method

It is true that if the single scattering approximation is not given in a layer, that layer has a too high optical thickness. However, the optical thickness is not the right variable for this optimization because the reverse is not true. If a layer has a high optical thickness, this can be the result of strong absorption, strong scattering or both. In cases where the absorption is high, the probability that radiation is scattered twice in a layer is very low, even if the scattering is strong. In this case, the single scattering approximation is valid, even if the optical thickness is very high. Only if the scattering is much stronger than the absorption, the single scattering approximation is not valid. The single scattering albedo $\omega$ quantifies the relation of scattering and absorption. It is defined as

$$\omega = \frac{\sigma}{\kappa} = \frac{\sigma}{\sigma + \alpha}. \tag{25}$$

If the scattering in one layer is much stronger than the absorption, $\omega$ is close to 1. If the scattering is small compared to the absorption, $\omega$ is close to 0. Figure 11 shows that the difference between DISORT and DOIT is indeed growing in regions where $\omega$ is high. It

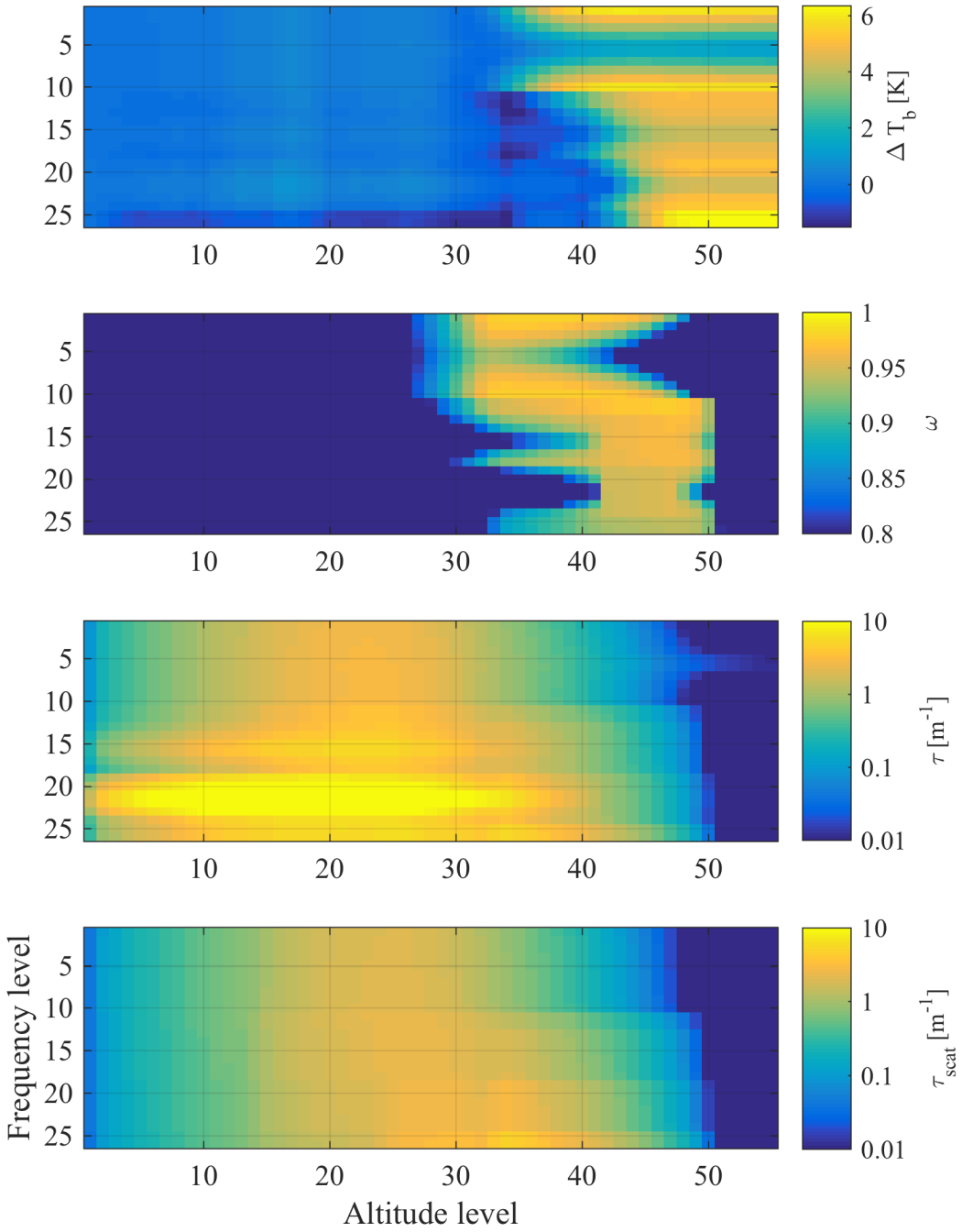


Figure 11: Difference between DOIT and DISORT of simulated brightness temperatures (top), single scattering albedo $\omega$ (middle top), optical thickness $\tau$ (middle bottom) and scattering optical thickness $\tau_{scat}$ (bottom) for 26 different frequencies and 56 different pressure levels

also shows that the error of DOIT does not depend on the optical thickness. Thus the optimization is only necessary in layers where $\omega$ is close to 1. The maximum allowed $\omega$, $\omega_{crit}$, can be set by the user. In chapter 4.3 the right choice of this value is discussed. In layers where $\omega$ is higher than this maximum value, the optimization needs to reduce the layer thickness in order to minimize the chance of radiation being scattered twice or more times in this layer. This should be oriented on the scattering. A good measure of the scattering in a layer is the scattering optical thickness $\tau_{scat}$ which is also displayed in Figure 11 and which only depends on the scattering coefficient:

$$\tau_{scat}(s_1, s_2) = \int_{s_1}^{s_2} \sigma(s')ds', \tag{26}$$

or in a homogeneous layer

$$\tau_{scat}(s_1, s_2) = \sigma(s_2 - s_1). \tag{27}$$

The user can again set a threshold, $\tau_{scat,crit}$, which is used to optimize the layer if this threshold is surpassed.

## 4.3 Implementation in DOIT

To calculate the optical properties in a layer, it is necessary to calculate the average optical properties over all particles. They can be calculated using the extinction cross sections, the absorption cross sections and the particle number distribution (PND) of all the scattering particles and the absorption species. This data can be found in the atmospheric data of the radiative transfer problem. ARTS takes only the extinction, the absorption cross sections and the PND of the scattering particles as input. The averaged extinction coefficient $\langle\kappa\rangle$ can be calculated using the extinction cross sections $C_{ext}(d)$ and the number density $n_0(d)$ for all particles with radius $d$:

$$\langle\kappa\rangle = \int n_0(d')C_{ext}(d')dd'. \tag{28}$$

Likewise, the averaged absorption coefficient $\langle\alpha\rangle$ can be calculated using the absorption cross section $C_{abs}$:

$$\langle\alpha\rangle = \int n_0(d')C_{abs}(d')dd'. \tag{29}$$

Since the extinction coefficient $\kappa$ is the sum of $\alpha$ and $\sigma$, $\langle\sigma\rangle$ can be calculated as

$$\langle\sigma\rangle = \langle\kappa\rangle - \langle\alpha\rangle \tag{30}$$

and in a medium with homogeneous layers, the scattering optical thickness follows from equation 27.

Now it is possible to calculate the single scattering albedo $\omega$ in all layers for every frequency using equation 25. This allows for the identification of those layers which need to be optimized by reducing the scattering optical thickness.
Because the scattering optical thickness depends on the thickness of the layers, it is useful to optimize the altitude grid. The pressure grid can then be optimized by interpolating it to the optimized altitude grid. In order to optimize the altitude grid, the scattering optical thickness in each layer is compared to the user-defined threshold. If the threshold $\tau_{scat,crit}$ is surpassed, new grid points are added using linear interpolation. For example, consider a layer of height $\Delta z$ where the scattering optical thickness is surpassed by a factor of $n$:

$$\tau_{scat} = \sigma \Delta z = n \tau_{scat,crit} > \tau_{scat,crit}. \tag{31}$$

The optimization now adds $n$ equidistant grid points in the layer. As shown in Figure 12, this leads to $n+1$ sub-layers with equal height

$$\Delta z_{new} = \frac{\Delta z}{n+1} \tag{32}$$

and the scattering optical thickness in these layers is

$$\tau_{scat,new} = \sigma \Delta z_{new} = \sigma \frac{\Delta z}{n+1} = \frac{n}{n+1} \tau_{scat,crit} < \tau_{scat,crit} \tag{33}$$

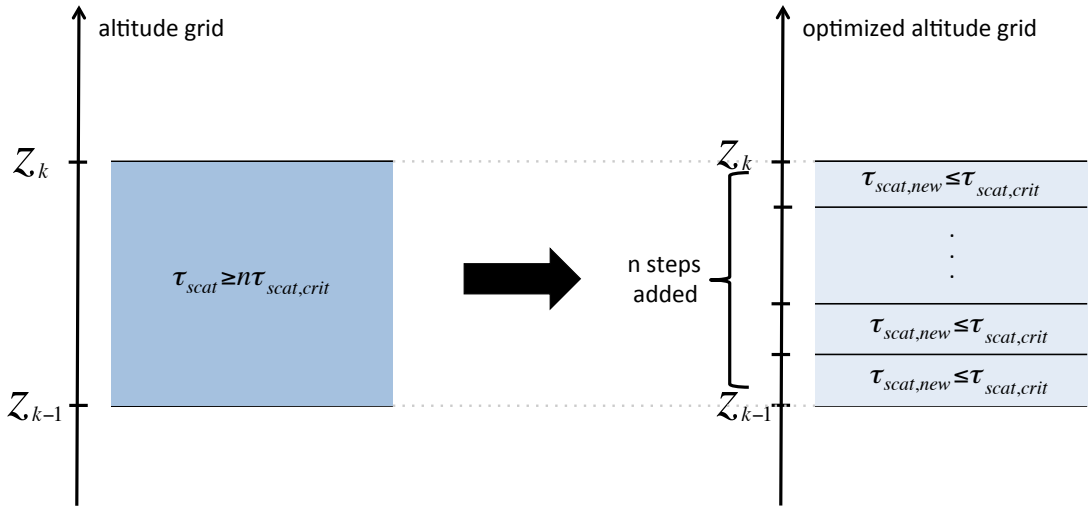


Figure 12: Visualization of the altitude grid optimization to reduce the scattering optical thickness

The pressure grid optimization therefore consists of three steps for every frequency: First, the single scattering albedo $\omega$ is calculated for every layer.
Second, layers where $\omega$ is above a given first threshold $\omega_{crit}$ are optimized by the optimization of the altitude grid, which calculates the scattering optical thickness $\tau_{scat}$ and divides the layers according to a second threshold $\tau_{scat,crit}$. The right choice of the two thresholds

will be discussed in the next section.
Third, the pressure grid and all other atmospheric fields are interpolated onto the new altitude grid. The scattering data is not calculated again but is instead interpolated, like the other fields. The errors arising from this interpolation are discussed in the next section. After the calculation, the calculated radiation field is interpolated back to the original grid, because the grid size has to be consistent for every frequency.
The optimization is implemented in ARTS and can be used by two workspace methods, *doit_p_gridOptimize*, which optimizes the grid for every frequency and interpolates the atmospheric fields, and *doit_Optimize_interp_i_field*, which interpolates the calculated radiation field back to the original pressure grid. The two thresholds can be set by the user.

## 4.4 Testing

To test the optimization method, the calculations described in section 4.1 are repeated with the optimized DOIT method. The right choice of the two thresholds is critical because there is a trade-off between accuracy and computation time. Two combinations are tested for the Chevallier atmosphere. One combination focuses more on accuracy whereas the other focuses on speed, i.e. not slowing down the calculation too much with a large pressure grid. The thresholds of both combinations as well as their average pressure grid enhancement are shown in table 2.

Table 2: Optimization thresholds and a factor which describes the average new size of the pressure grid relative to the old grid, for the two tested combinations

| Combination | $\omega_{crit}$ | $\tau_{scat,crit}$ | Factor of grid enhancement |
|---|---|---|---|
| "accuracy" | 0.9 | 0.1 | 3 |
| "speed" | 0.9 | 0.2 | 2 |

Figure 13 shows that both combinations lead to a significant decrease of the model differences. While the combination "speed" manages to reduce the difference to below 2 K, the combination "accuracy" manages to reduce the differences even further, to at or below 1 K. Both combinations, however, take much more time to calculate because of the finer pressure grid. Furthermore, in the optimized calculations, DOIT takes a few more iterations to converge. This is probably caused by the need to simulate more scattering with a finer pressure grid. The scattering processes inside the original pressure levels which are neglected because of the single scattering approximation are now simulated as scattering between the finer pressure levels.
Because the combination "accuracy" leads to more accurate results, its thresholds are set as the default thresholds of the method. However, the user can change those thresholds as he pleases.
In order to estimate the errors that arise from the interpolation, the results of the optimized DOIT are compared to a manual optimization. For the manual optimization, the optimized pressure grid is calculated externally and then DOIT is started with that pressure grid. This

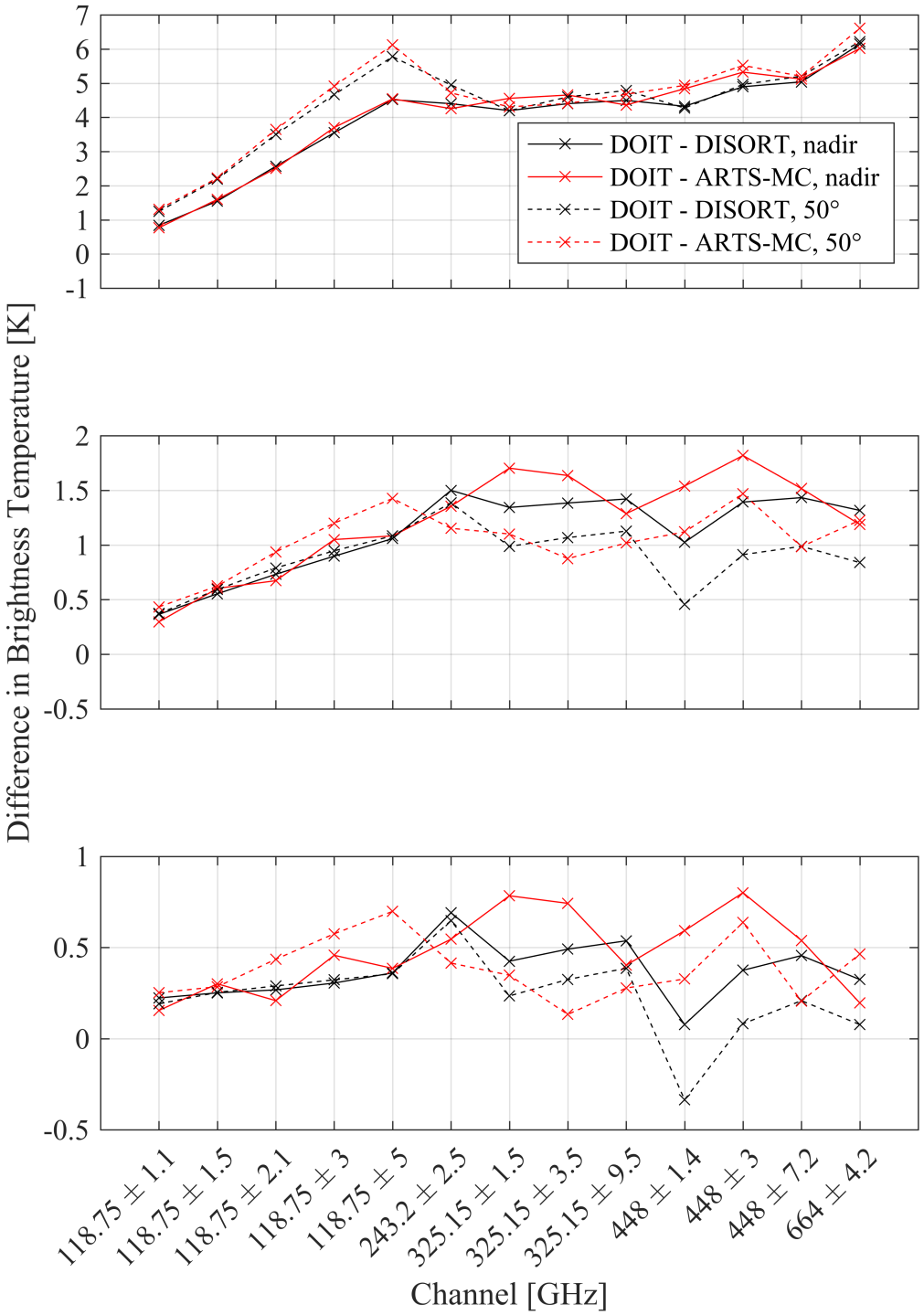


Figure 13: Difference of DOIT to DISORT and ARTS-MC in simulated brightness temperatures for 13 different channels for the non-optimized DOIT (top) the combination “speed” (middle) and the combination “accuracy” (bottom)

way, the scattering data is calculated directly with the optimized pressure grid. However, the differences to the internal optimization are below 0.1 K and can thus be neglected.
The above mentioned atmosphere from the Chevallier data set is a rather extreme test case. To test the optimization in a less extreme environment, calculations are done using 306 atmospheres of the Eresmaa data set (Eresmaa and McNally, 2014). The atmospheres are randomly chosen from the whole data set of atmospheric profiles. The calculations are done without and with optimization. For the optimization, the discussed default combination of thresholds is used. The results are only compared to DISORT, because ARTS-MC takes too much time with an accuracy of 0.1 K. Figure 14 shows that without optimization, the difference to DISORT is quite high in some atmospheres and channels. However, the optimization is able to reduce these differences to a maximum of around 1 K.

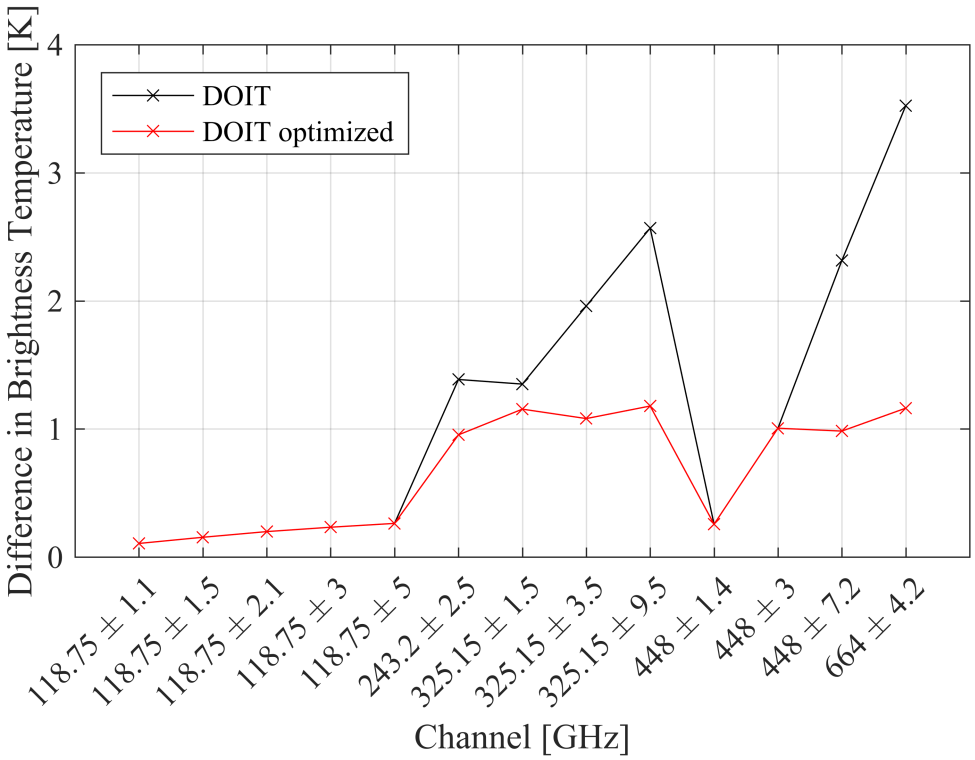


Figure 14: Maximum differences over 306 atmospheres in the simulated brightness temperatures of DOIT and the optimized DOIT to DISORT for 13 channels, looking nadir

A difference of 1 K is acceptable because it is within the measurement error of current remote sensing instruments. The accuracy of MARSS, for instance, is around 1 K according to McGrath and Hewison (2001).
For a few atmospheres of this test, however, the optmization expands the pressure grid by a large factor, leading to very large computation times. This means that the results are accurate, but they take an unacceptable time to calculate.

# 5 Summary and Conclusion

This thesis has been motivated by two issues of the DOIT scattering solver. The first issue is the slow convergence. To attack this issue, the Ng-acceleration was described, implemented into DOIT and tested. The implementation of the Ng-acceleration was successful. It clearly showed an accelerating effect on the radiative transfer calculations as it reduced the number of iterations by about 10% in the test cases. Its effect was however only visible where the non-accelerated version takes more than 5 iterations in the first place. In those cases, the effect was stronger the more iterations are needed to reach convergence. This means that the accelerated version has a great advantage over the non-accelerated version in difficult atmospheres, i.e. atmospheres with a lot of snow and ice.
Furthermore, the acceleration worked for polarized as well as for unpolarized radiation. The effect was slightly smaller for polarized radiation as the convergence behavior in the last three components of the Stokes vector is more difficult for the acceleration method. The accelerated version lead to the same results as the non-accelerated. It even reduced the number of cases where the process is converged but the result is far from the reference solution.
So far, the Ng-acceleration has only been implemented to the 1-dimensional version of DOIT. A subject of further development is to extend the acceleration to the 3-dimensional version.
The second issue is the significant difference which DOIT showed in comparison to other scattering solvers, DISORT and ARTS-MC. The analysis showed that the difference resulted from a too coarse resolution of the pressure grid. A method to optimize the pressure grid based on the single scattering albedo and the scattering optical thickness was introduced, implemented to DOIT and tested.
The tests have shown that the implemented pressure grid optimization is capable of reducing the differences of DOIT to other scattering solvers from up to 6 K to around 1 K in some extreme cases. This is an acceptable difference as it is in the range of current radiation measurement errors. The optimization comes at the cost of a greater calculation time because of the enhanced pressure grid. To avoid unacceptably long calculation times, there should be a limitation to the optimization. This feature would allow the user to set a maximum pressure grid size. It will be subject to further development.
Another source of error is the resolution of the angular grid in DOIT. In thie thesis, these errors were suppressed by a very fine angular grid. This strongly increased the calculation time in the tests. A better solution would be an angular grid optimization which only enhances the angular grid when necessary. This optimization will be tackled by following works.

# Appendices

## A Derivation of a and b in the Ng-acceleration

The derivation starts with the problem of the form

$$f_{n+1} = Af_n, \tag{34}$$

where $f_{n+1}$ and $f_n$ are two successive iterations of $f$. Given the iterations $f_n, f_{n-1}, f_{n-2}$ and $f_{n-3}$, $\bar{f}_1$ is defined as

$$\bar{f}_1 = (1-a-b)f_{n-1} + af_{n-2} + bf_{n-3} \tag{35}$$

and its successor $\bar{f}_2$ as

$$\bar{f}_2 = (1-a-b)f_n + af_{n-1} + bf_{n-2}, \tag{36}$$

where $a$ and $b$ are some constants to be determined. Because $\bar{f}_2$ is the successor of $\bar{f}_1$, it is possible to write

$$\bar{f}_2 = A\bar{f}_1. \tag{37}$$

The difference $d$ between $\bar{f}_2$ and $\bar{f}_1$ is defined as

$$d = \bar{f}_2 - \bar{f}_1 = A\bar{f}_1 - \bar{f}_1. \tag{38}$$

$d$ can be rewritten as

$$\begin{aligned} d = \bar{f}_2 - \bar{f}_1 &= (1-a-b)f_n + af_{n-1} + bf_{n-2} - [(1-a-b)f_{n-1} + af_{n-2} + bf_{n-3}] \\ &= f_n - f_{n-1} - a(f_n - 2f_{n-1} + f_{n-2}) - b(f_n - f_{n-1} - f_{n-2} + f_{n-3}) \\ &= d_n - ad_1 - bd_2 \end{aligned} \tag{39}$$

with

$$d_n = f_n - f_{n-1} \tag{40}$$

$$d_1 = f_n - 2f_{n-1} + f_{n-2} \tag{41}$$

$$d_2 = f_n - f_{n-1} - f_{n-2} + f_{n-3}. \tag{42}$$

Because $\bar{f}_2$ is the successor of $\bar{f}_1$, the difference $d$ between the two will get very small as the process approaches convergence. A good measure of the difference $d$ is the norm which has been introduced in equation 14 in chapter 2.3. In order to accelerate the iterative process, it is necessary to minimize $||d||_2^2$ with respect to $a$ and $b$ by taking the derivative with respect to $a$ and $b$ and setting it zero. The squared norm of $d$ is given by (omitting

dependencies on the integration variable $x$)

$$\begin{aligned} ||d||_2^2 &= \int_D d^2 dx = \int_D (d_n - ad_1 - bd_2)^2 dx \\ &= \int_D (d_n^2 - 2ad_n d_1 - 2bd_n d_2 + a^2 d_1^2 + b^2 d_2^2 + 2abd_1 d_2) dx \end{aligned} \tag{43}$$

where $D$ is the domain of $f$. When taking the derivative with respect to $a$ of the above, the integral and the derivative can be switched . This is possible because the integration is over $x$ while the derivative is with respect to $a$. Both are independent from each other. Taking the derivative with respect to $a$ leads to

$$\begin{aligned} \frac{d}{da}||d||_2^2 &= \int_D \frac{d}{da}(d_n^2 - 2ad_n d_1 - 2bd_n d_2 + a^2 d_1^2 + b^2 d_2^2 + 2abd_1 d_2) dx \\ &= \int_D (-2d_n d_1 + 2ad_1^2 + 2bd_1 d_2) dx \stackrel{!}{=} 0. \end{aligned} \tag{44}$$

This integral can be split up into three integrals. The constants $a$ and $b$ can be pulled out of the integrals and the integrals can be written in the form of the scalar product defined in equation 17 in section 3.3:

$$\begin{aligned} \frac{d}{da}||d||_2^2 &= -2\int_D d_n d_1 dx + 2a\int_D d_1^2 dx + 2b\int_D d_1 d_2 dx \\ &= -2(d_n, d_1) + 2a(d_1, d_1) + 2b(d_1, d_2) \stackrel{!}{=} 0. \end{aligned} \tag{45}$$

This equation can be divided by 2 to get

$$-(d_n, d_1) + a(d_1, d_1) + b(d_1, d_2) \stackrel{!}{=} 0. \tag{46}$$

Similarly, taking the derivative of $||d||_2^2$ with respect to $b$ leads to a second equation:

$$-(d_n, d_2) + b(d_2, d_2) + a(d_1, d_2) \stackrel{!}{=} 0. \tag{47}$$

Equations 46 and 47 can be used to solve for $a$ and $b$. The results is

$$a = \frac{(d_n, d_1)(d_2, d_2) - (d_n, d_2)(d_1, d_2)}{(d_1, d_2)(d_2, d_2) - (d_1, d_2)(d_1, d_2)} \tag{48}$$

$$b = \frac{(d_n, d_1)(d_1, d_2) - (d_n, d_2)(d_1, d_1)}{(d_1, d_2)(d_1, d_2) - (d_2, d_2)(d_1, d_1)} \tag{49}$$

The accelerated field

$$\bar{f_2} = (1 - a - b)f_n + af_{n-1} + bf_{n-2} \tag{50}$$

is chosen as the (n+1)-th iteration.

# B Additional figures for polarized radiation

Below are figures of the performance of the Ng-acceleration for polarized radiation.

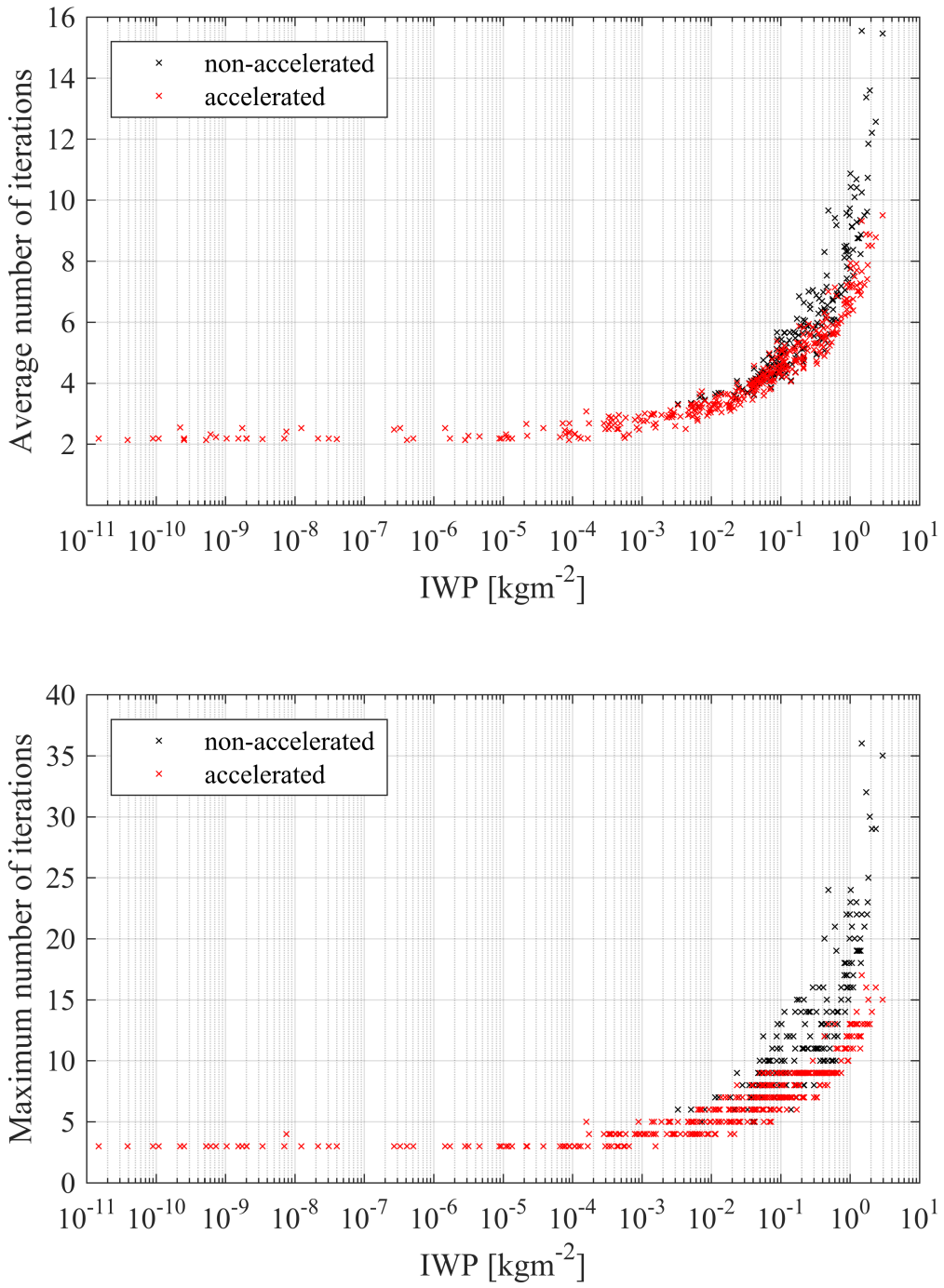


Figure 15: Number of iterations until convergence, for all atmospheres, average (top) and maximum (bottom) over all frequencies, for the non-accelerated and the accelerated version of DOIT against the IWP in the atmosphere; polarized radiation

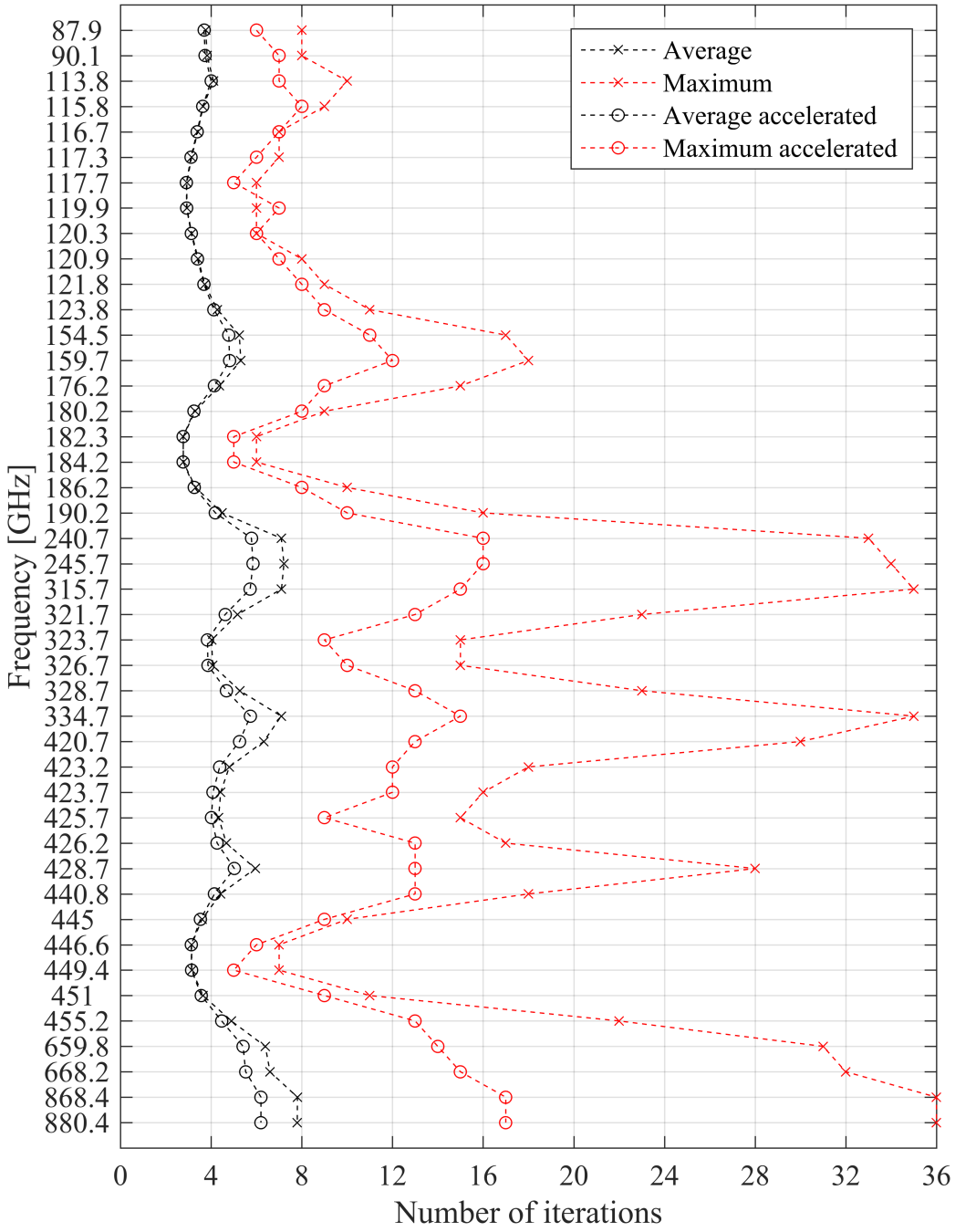


Figure 16: Average and maximum iterations over all atmospheres with respect to the frequency of the 44 channels for the accelerated and the non-accelerated version of DOIT, calculation with polarized radiation

## References

Buehler, S. A., Eriksson, P., Kuhn, T., von Engeln, A., and Verdes, C. ARTS, the atmospheric radiative transfer simulator. *JQSRT*, 91(1):65–93, feb 2005. doi: 10.1016/j.jqsrt.2004.05.051.

Buehler, S. A., Jiménez, C., Evans, K. F., Eriksson, P., Rydberg, B., Heymsfield, A. J., Stubenrauch, C., Lohmann, U., Emde, C., John, V. O., Sreerekha, T. R., and Davis, C. P. A concept for a satellite mission to measure cloud ice water path and ice particle size. *QJRMS*, 133(S2):109–128, 2007. doi: 10.1002/qj.143.

Chevallier, F., Di Michele, S., and McNally, A. P. Diverse profile datasets from the ECMWF 91-level short-range forecasts. Technical report, NWP SAF, 2006.

Davis, C., Emde, C., and Harwood, R. A 3-d polarized reversed monte carlo radiative transfer model for millimeter and submillimeter passive remote sensing in cloudy atmospheres. *IEEE Transactions on Geoscience and Remote Sensing*, 43(5):1096–1101, 2005.

Emde, C., Buehler, S., Davis, C., Eriksson, P., Sreerekha, T., and Teichmann, C. A polarized discrete ordinate scattering model for simulations of limb and nadir long-wave measurements in 1-d/3-d spherical atmospheres. *Journal of Geophysical Research*, 109, 2004.

Eresmaa, R. and McNally, A. P. Diverse profile datasets from the ECMWF 137-level short-range forecasts. Technical report, NWP SAF Satellite Application Facility for Numerical Weather Prediction, Oct. 2014.

Eriksson, P., Buehler, S. A., Davis, C. P., Emde, C., and Lemke, O. ARTS, the atmospheric radiative transfer simulator, version 2. *JQSRT*, 112(10):1551–1558, 2011. doi: 10.1016/j.jqsrt.2011.03.001.

Eriksson, P., Buehler, S., Emde, C., and Lemke, O. *ARTS 2-2-59 User Guide*. University of Hamburg, Hamburg, Germany, 2016. (Available at http://www.radiativetransfer.org/misc/arts-doc-stable/uguide/arts˙user.pdf).

Evans, K. F., Wang, J. R., Starr, D. O., Heymsfield, G., Li, L., Tian, L., Lawson, R. P., Heymsfield, A. J., and Bansemer, A. Ice hydrometeor profile retrieval algorithm for high-frequency microwave radiometers: application to the CoSSIR instrument during TC4. *AMT*, 5(9):2277–2306, 2012. doi: 10.5194/amt-5-2277-2012.

Fox, S., Lee, C., Rule, I., King, R., Rogers, S., Harlow, C., and Baran, A. ISMAR: A new submillimeter airborne radiometer. In *2014 13th Specialist Meeting on Microwave Radiometry and Remote Sensing of the Environment (MicroRad), Proceedings*, pages 128–132, 2014. doi: 10.1109/MicroRad.2014.6878923.

Geer, A. J. and Baordo, F. Improved scattering radiative transfer for frozen hydrometeors at microwave frequencies. *AMT*, 7:1839–1860, 2014. doi: 10.5194/amt-7-1839-2014.

Hong, G., Yang, P., Baum, B. A., Heymsfield, A. J., Weng, F., Liu, Q., Heygster, G., and Buehler, S. A. Scattering database in the millimeter and submillimeter wave range of 100–1000 GHz for nonspherical ice particles. *JGR*, 114:D06201, 2009. doi: 10.1029/2008JD010451.

Liu, Q., Weng, F., and Englisch, S. An improved fast microwave water emissivity model. *IEEE transactions on geoscience and remote sensing*, 49(4):1238–1250, 2011.

McGrath, A. and Hewison, T. Measuring the accuracy of MARSS- an airborne microwave radiometer. *JAOT*, 18:2003–2012, 2001.

Mishchenko, M. I., Travis, L. D., and Lacis, A. A. *Scattering, Absorption and Emission of Light by Small Particles*. Cambridge Univ. Press., New York, 2002.

Mlawer, E. J., Payne, V. H., Moncet, J.-L., Delamere, J. S., Alvarado, M. J., and Tobin, D. C. Development and recent evaluation of the MT_CKD model of continuum absorption. *PTRSA*, 370(1968):2520–2556, 2012. doi: 10.1098/rsta.2011.0295.

Ng, K.-C. Hypernetted chain solutions for the classical one-component plasma up to $\Gamma = 7000$. *Journal of Chemical Physics*, page 2680, 1974.

Olson, G., Auer, L., and Buchler, J. A rapidly convergent iterative solution of the non-lte line radiation transfer problem. *Journal of Quantitative Spectroscopy and Radiative Transfer*, 35(6):432 – 442, 1986.

Pereira, T. and Uitenbroek, H. Rh 1.5d: a massively parallel code for multi-level radiative transfer with partial frequency redistribution and zeeman polarisation. *Astronomy and Astrophysics*, 574, 2015.

Pica, G., Alberti, G., Memoli, A., Santovito, M. R., Varchetta, S., Buralli, B., D'Addio, S., and Kangas, V. MetOp Second Generation: A joint ESA/EUMETSAT mission for weather forecast and climate monitoring with an imaging radiometer. In *Proceedings of the 63rd International Astronautical Congress 2012 (IAC 2012)*, pages 3132–3136. International Astronautical Federation (IAF), 2012. paper: IAC-12-B1.3.10.

Rees, W. G. *Physical Principles of Remote Sensing*. Cambridge Univ. Press, Cambridge, 2012.

Reinert, D., Prill, F., Frank, H., and Zängl, G. *ICON Database Reference Manual*. Deutscher Wetterdienst, 2016. Version 1.1.8.

Rothman, L. S., Gordon, I. E., Babikov, Y., Barbe, A., Benner, D. C., Bernath, P. F., Birk, M., Bizzocchi, L., Boudon, V., Brown, L. R., Campargue, A., Chance, K., Cohen, E. A., Coudert, L. H., Devi, V. M., Drouin, B. J., Fayt, A., Flaud, J.-M., Gamache, R. R., Harrison, J. J., Hartmann, J.-M., Hill, C., Hodges, J. T., Jacquemart, D., Jolly, A., Lamouroux, J., Le Roy, R. J., Li, G., Long, D. A., Lyulin, O. M., Mackie, C. J., Massie, S. T., Mikhailenko, S., Müller, H. S. P., Naumenko, O. V., Nikitin, A. V., Orphal, J., Perevalov, V., Perrin, A., Polovtseva, E. R., Richard, C., Smith, M. A. H., Starikova, E., Sung, K., Tashkun, S., Tennyson, J., Toon, G. C., Tyuterev, V. G., and Wagner, G. The HITRAN2012 molecular spectroscopic database. *JQSRT*, 130:4–50, 2013. doi: 10.1016/j.jqsrt.2013.07.002.

Saunders, R. W., Hewison, T. J., Stringer, S. J., and Atkinson, N. C. The radiometric characterization of AMSU-B. *I3ETMTT*, 43(4):760–771, 1995.

Stamnes, K., Tsay, S.-C., and Laszlo, I. DISORT, a general-purpose fortran program for discrete-ordinate-method radiative transfer in scattering and emitting layered media: Documentation of methodology. Technical report, Dept. of Physics and Engineering Physics Stevens Institute of Technology,NASA Goggard Space Flight Center, Department of Meteorology University of Maryland, 2000.

Stratton, J. A. *Electromagnetic Theory*. McGraw-Hill Book Company, Inc., New York, 1941.

Zängl, G., Reinert, D., Rípodas, P., and Baldauf, M. The ICON (ICOsahedral Non-hydrostatic) modelling framework of DWD and MPI-M: Description of the non-hydrostatic dynamical core. *QJRMS*, 141(687):563–579, 2015. doi: 10.1002/qj.2378.

## Acknowledgments

I would like to thank everyone who has been supporting me in writing this thesis.
I would like to thank Oliver Lemke for his support with the implementation of the methods in ARTS.
I would like to thank the members of the group *Radiation and Remote Sensing* for interesting and helpful conversations on the topic of this thesis, especially Simon Michel, Theresa Lang and Marc Prange.
I would like to thank Laura Dietrich who has been helping me with suggestions and corrections throughout the entire process of writing this thesis.
I would like to thank Gabi Wolter for correcting the grammatical errors in this thesis.
Furthermore I would like to thank Stefan Buehler for introducing me to and letting me work on this interesting matter.
Last but not least I would like to thank Manfred Brath who has been supporting me the whole time. I apologize to him for asking many questions on seemingly unimportant matters, but he never rejected to answer me. This has helped me a lot.

## Eidesstattliche Erklärung

Ich versichere an Eides statt, dass ich die Arbeit selbstständig verfasst und keine anderen als die angegebenen Hilfsmittel verwendet habe. Insbesondere habe ich keine im Quellenverzeichnis nicht genannte Internet-Quellen benutzt. Zudem versichere ich, dass ich die Arbeit vorher nicht in einem anderen Prüfungsverfahren eingereicht habe und dass die eingereichte schriftliche Fassung der auf dem elektronischen Speichermedium entspricht.

| | |
|---|---|
| Ort, Datum | Jakob Dörr |